THE JOURNAL OF PHYSICAL CHEMISTRY C

pubs.acs.org/JPCC Article

Transition Zone Theory Compared to Standard Models: Reexamining the Theory of Crystal Growth from Melts

James D. Martin,* Berkley G. Hillis, and Feier Hou

Cite This: J. Phys. Chem. C 2020, 124, 18724–18740

Read Online

ACCESS | Metrics & More | Article Recommendations

ABSTRACT: Ideas proposed at the beginning of the 20th century to describe the temperature dependence of crystal growth rates have become accepted as the "standard model." Specifically, it was proposed that rates are controlled by a thermodynamic driving force, liquid/solid interfacial surface energy requires crystal growth to occur at step or kink sites, and particle diffusion/viscous relaxation also controls the rate of growth. However, as described in this article, these underlying assumptions are inconsistent with the fact that crystal growth from supercooled melts is microscopically irreversible, and the well-known fact that short- and intermediate-range order in melts and crystals is essentially equivalent, precluding the existence of sharp interfaces and the need for material diffusion. By contrast, we recently introduced the Transition Zone Theory of crystallization, TZT_c, a condensed matter analogue of Eyring's transition state theory that uses Kauzmann's conception of configurational entropy and Adam and Gibbs' ideas of cooperativity to describe the ensemble characteristics governing crystal growth rates. Here, the TZT_c model is applied to the same sets of inorganic oxides and organic molecules that were used to evaluate the apparent decoupling of viscosity from the standard model, as well as to several other materials. Without exception, the TZT_c model provides a superior fit to temperature-dependent crystal growth-rate data. With a single model accurately describing diverse crystallizing systems, the three parameters extracted from TZT_c, for the first time, provide a platform with which to compare and contrast chemical/physical factors that influence crystallization reactions.

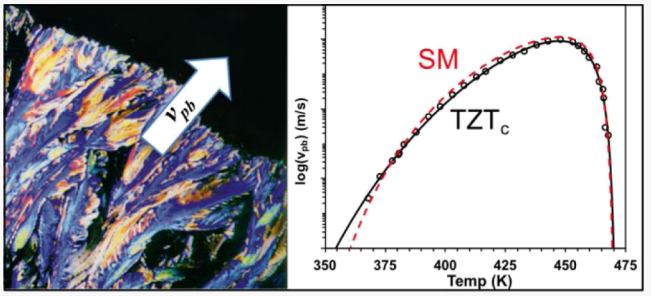

1. INTRODUCTION

Crystallization is one of the earliest chemical processes studied by humans, with evidence that salt crystallization from seawater was practiced in prehistoric times. An insightful history of efforts to understand the process(es) of crystal growth is reviewed by Bohm.[1] Possibly the first atomic/molecular-type mechanistic model of crystal growth was Kepler's 1611 description of snowflakes being built by the assembly of close-packed spherical particles.[2] Throughout the 19th and 20th century, the requirement for supercooling or supersaturation was clearly documented.[3,4,5] Gibbs' theoretical work in the 1870s describing heterogeneous equilibria began to establish quantitative principles for crystal growth.[6]

Like the over-extrapolation of Kepler's microscopic observations of snowflake shapes into microscopic presumptions of particle-based assembly, the macroscopic observation that crystallization requires supercooling/supersaturation, and a physically observable sharp boundary between a crystal and the gas or liquid from which it grows, also has been over-extrapolated in atomistic/molecular descriptions of crystal growth processes. Nevertheless, these assumptions dominate most modern crystallization models. Specifically, supercooling and equilibrium concepts form the basis of descriptions of a driving force for crystallization (the driving force assumption). The perceived need to transport material across a liquid (gas) interface to the growing crystal forms the basis for the assumptions that particles exist as either a liquid (gas) or a crystal (the individual particle assumption) and that particle diffusion and/or a material's viscosity controls growth rates (the diffusion/viscosity assumption). The concepts of diffusion/viscosity and a driving force have been used to explain why crystal nucleation and growth rates increase to a maximum, T_{max}, and then diminish with greater extents of supercooling.[3−5,7]

The principles of the driving force, surface energy, and material diffusion at the root of classical models of crystal growth were derived for crystallization from the gas phase or dilute solutions but are routinely applied to describe melt crystallization. Although conceptually treated in the literature as established fact, the literature is replete with examples where

Received: April 4, 2020
Revised: June 15, 2020
Published: June 25, 2020

classical models only fit observed experimental data over limited temperature ranges unless substantial modifications are introduced.[8−10] Rather than further modifying existing models, we propose that understanding of the cooperative, ensemble nature of condensed matter requires reconsideration of the fundamental individual particle-based assumptions, particularly with respect to understanding crystal growth in congruently melting systems.

In this article, we begin with (Section 2) a summary of the development of classical models of crystal growth rates and then (Section 3) reexamine fundamental assumptions of thermodynamics and kinetics in light of these models. We then introduce our recently discovered transition zone theory of crystallization (TZT_c),[11] which, consistent with principles of kinetics and thermodynamics, integrates the principles of configurational entropy (Kauzmann[12]) and cooperativity (Adam and Gibbs[13]) into the principles of Eyring's transition state theory[14] (Section 4). The TZT_c is then applied to evaluate the experimental crystal growth rate data for the same set of diverse materials previously evaluated by Nascimento et al.[15] and Ediger et al.[8] to consider apparent viscosity decoupling, as well as to several additional materials (Section 5). Finally, we apply the understanding of temperature-dependent configurational entropy and cooperativity to re-evaluate the apparent correlation/decoupling between viscous relaxation and crystal growth rates (Section 6).

2. SUMMARY OF CLASSICAL MODELS

To describe the temperature-dependent rate of crystal growth, Wilson introduced eq 1,[4] which quantitates crystallization assumptions of a driving force, an interface of distinct liquid and crystalline particles, and that particles must be transported to and across that growing interface.

$$v = C\frac{s}{V} \tag{1}$$

where v is the velocity of solidification, C is a constant related to the heat of fusion and the thickness of a layer of molecules at the interface, V is the viscosity of the liquid, and s is the actual supercooling. In Wilson's model, the driving force assumption is quantified as the extent of supercooling. Based on experimental measurements of both viscosity and crystal growth rates, he concluded that eq 1 "represents the variation of v with s sufficiently well to justify the conclusion that the [crystal growth] velocity is largely determined by the viscosity."[4]

Volmer subsequently advanced a molecular transition state theory-type approach to crystal growth, suggesting the rate of crystal growth to be related to the balance between the energy required to break bonds from the liquid to pass into the lattice and the energy required to break bonds of the solid to pass to the liquid.[16] Thus, he suggested that at the melting point, $Q_1 = Q_s + Q_2$, where Q_1 and Q_2 are the activation energies for detaching from the solid and liquid, respectively, and Q_s is the heat of fusion. Setting the rates of crystallization and melting to be equal at the melting temperature (described then as T_s as opposed to the modern description as T_m), he proposed eq 2

$$v = K\exp\left(\frac{-Q_1}{RT}\right)\left(\exp\left(\frac{Q_s(T_s - T)}{RTT_s}\right) - 1\right) \tag{2}$$

where K is a proportionality constant and R is the gas constant. It is important to note that setting the rates of crystallization and melting to be equivalent presumes that the processes are microscopically reversible, which is only the case precisely at the melting or liquidous temperature where the chemical potential of the liquid and crystal are equivalent, $\mu_l = \mu_s$.

Physical observation of crystal growth of Hg grown from the saturated vapor, Cd and Sn grown electrolytically, and PbI_2 grown from the precipitation reaction of $PbNO_3$ and KI, however, demonstrated crystal growth that seemed to be faster across a given layer than the rate of layer propagation.[17] Kossel recognized that thermodynamic equilibrium provided an incomplete basis to describe such crystal growth and proposed a model that recognized different energies of attachment depending on whether a particle attaches to a face, an edge, or a kink site.[18] To address both growth of a given network layer and the emergence of new network layers, Volmer introduced an alternative expression to describe crystal growth velocity, eq 3

$$v = A\exp\left(\frac{-Q_1}{RT}\right)\exp\left(\frac{\pi\rho^2 FT_s}{KQ_sT(T_s - T)}\right) \tag{3}$$

where A and K are material-specific proportionality constants, F is the face size, ρ is a free energy of the growth boundaries, Q_1 is activation energy, and Q_s is the energetic difference between melt and crystalline phases at the melting point.[16] Eq 3 provided a somewhat better fit to the experimental data for crystallization of glycerin from the melt than did eq 2. Although both models capture the general form of temperature-dependent growth rates, neither provides a good quantitative fit.

Subsequent work of, for example, Frenkel,[5] Becker and Döring,[7] Turnbull and Fisher,[19] Cahn,[20] and Jackson, Uhlmann, and Hunt,[21] integrated the ideas that the rate of crystal growth is controlled by the free-energy difference between the two phases and the rate at which molecules can diffuse to and organize into a crystal (a function of the viscosity and nature of the interface) into what is generally described as the standard or normal model, eqs 4 and 5.

$$U = f\frac{D}{\lambda}\left[1 - \exp\left(\frac{\Delta G}{k_BT}\right)\right] \tag{4}$$

where U is the observed growth rate, f is a function that describes the available attachment sites, D is the diffusion coefficient, ΔG is the free-energy difference between liquid and crystalline phases said to be the driving force of crystallization, and λ is the "jump distance" of the advancing interface. The diffusion coefficient is most commonly expressed in terms of the Stokes−Einstein/Eyring (SE/E) relationship,[5] giving eq 5.

$$U = f\frac{k_BT}{\lambda^2\eta}\left[1 - \exp\left(\frac{\Delta G}{k_BT}\right)\right] \tag{5}$$

where η is the shear viscosity.[21]

To describe distinct models of growth at the liquid/crystal interface, the function f may be set equal to one to describe continuous growth of the normal or standard model. Alternatively, the screw dislocation growth model, eq 6, or the two-dimensional (2-D) surface nucleation growth model, eq 7, are commonly employed.[21]

$$U = \frac{k_BT\Delta G}{4\pi\gamma V_m\lambda\eta}\left[1 - \exp\left(\frac{\Delta G}{k_BT}\right)\right] \tag{6}$$

https://dx.doi.org/10.1021/acs.jpcc.0c03003
J. Phys. Chem. C 2020, 124, 18724−18740

where γ is the specific surface energy of the liquid/crystal interface and V_m is the molar volume of the crystal.

$$U = \left(\exp\left(\frac{\pi\lambda V_m\gamma^2}{3k_BT\Delta G}\right)\right)\left(\frac{k_BT}{\lambda^3\eta}\right)\frac{\sqrt[3]{\pi N_s\lambda^5/3}}{\Gamma(4/3)}\left[1-\exp\left(\frac{-\Delta G}{RT}\right)^{2/3}\right] \quad (7)$$

where N_s is the number of formula units per unit area of interface and Γ is the gamma function.

Jackson et al. suggested consideration of a reduced growth rate, $U_R = U\eta/[1 - \exp(-\Delta G/RT)]$, that can be used to differentiate growth models corresponding to smooth (screw or 2-D) versus rough (normal) interfaces.[21] Differentiating between these models, however, is largely accomplished by evaluating which model best fits the experimental data, rather than the existence of specific experimental observables that distinguish normal, screw, or 2-D growth. However, while providing reasonable fits to the data, we find it to be chemically/physically surprising that, for example, $Li_2O{\cdot}2SiO_2$, $Li_2O{\cdot}3SiO_2$, and $Na_2O{\cdot}2SiO_2$, which all share a common layered silicate crystalline structure, are reported to crystallize according to hybrid (screw + 2-D), 2-D, and screw growth models, respectively.[15] Is there distinct chemistry? Or are the models incomplete?

Experimentally, it is observed that at deep supercooling, and particularly for fragile liquids, there is a significant deviation between experimental and standard model growth rates, suggested to be a result of decoupling of the diffusion coefficient from viscosity.[8−10,15] Similar to the multiple proposed interface models, various models are proposed to address the apparent viscosity-decoupling. Ediger et al. proposed that the reduced growth rate U_R, otherwise described as u_{kin}, is proportional to η^{ξ} where ξ is a parameter obtained from the slope of the $\log(u_{kin})$ versus $\log(\eta)$ plot.[8] Alternatively, Schmelzer et al. identified a decoupling temperature, T_D, below which they suggest addition of an Arrhenian term $(D_0\exp(-E_a/RT))$ into the classical diffusion equation.[9] Cassar et al. further modified this conception to describe a gradual transition from viscosity controlled to Arrhenian controlled diffusion.[10]

Notably, the suggestion to introduce an Arrhenian term into the classical diffusion equation is reminiscent of efforts to correct the classical Volger−Folcher−Tamman (VFT) equation for viscosity[22−24] with the introduction of an arbitrary crossover temperature between VFT and Arrhenius rate laws.[25,26] Mauro, however, recently suggested the apparent dynamic divergence of diffusion and viscosity is an artifact of the VFT equation.[27]

The above noted requirement of three distinct models to describe crystallization of the single structural family of alkali silicates, and the question of whether the decoupling of viscosity and diffusion at low temperature is real or an artifact, suggested to us that it may be necessary to reconsider the fundamental assumptions at the root of the classic models (i.e., driving force, independent particle, and diffusion/viscosity assumptions).

3. REEXAMINING FUNDAMENTAL ASSUMPTIONS

3.1. Driving Force Assumption. The concept of a "driving force" has been broadly associated with crystal growth models based on assumptions derived from equilibrium processes in dilute systems (i.e., gas phase or dilute solution). It is important to recognize, however, that even the early work of Kossel suggests that crystal growth processes are unlikely controlled by conditions of thermodynamic equilibrium.[18] Nevertheless, as noted above, Volmer described the energetics of a crystallizing system at the melting point, where the liquid and crystalline phases are in thermodynamic equilibrium, as $Q_1 = Q_s + Q_2$.[16] Rewriting in terms of the free energy of the reaction and free energies of activation for the forward $(\Delta G_f^{\ddagger})$ and reverse $(\Delta G_r^{\ddagger})$ directions, respectively, gives eq 8

$$\Delta G_r^{\ddagger} = \Delta G + \Delta G_f^{\ddagger} \quad (8)$$

for which at equilibrium, $\Delta G = 0$. If the crystalizing system is supercooled, ΔG_{rxn} becomes negative, thus increasing the "driving force" of the reaction. Mapping this onto a traditional reaction coordinate diagram[28] provides the description shown in Figure 1a, for which microscopic reversibility is presumed.

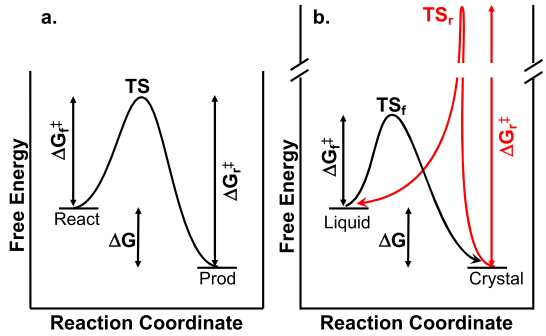

Figure 1. (a) Traditional reaction coordinate diagram based on the equilibrium assumption of microscopic reversibility. (b) Schematic reaction coordinate diagram representing the microscopic irreversibility of crystallization under supercooled conditions.

It is important to recognize that this classically described "driving force" is a thermodynamic parameter, ΔG, which has no direct correlation with the magnitude of the activation energy, $\Delta G^{\ddagger}$, of the reaction. For example, two reversible systems could have equivalent ΔG values with substantially different magnitudes of their activation energies, $\Delta G^{\ddagger}$'s. Nevertheless, it is worthwhile to consider both the conditions of reversibility of a phase transition and the nature of the activation energy for the reaction.

Reversibility of a reaction is defined by equilibrium conditions as determined by the second law of thermodynamics. At equilibrium, the chemical potential of a substance is the same throughout the sample, regardless of how many phases are present, and thus transition between phases at equilibrium is completely reversible. The chemical potential for a substance being $\mu = \frac{\partial G}{\partial n}$ indicates that for a pure substance, its chemical potential is equal to its molar Gibbs free energy, $\mu = G_m$. At equilibrium, $\Delta G = \Delta\mu = 0$, that is, there is no driving force at the reversible condition. The second law of thermodynamics also indicates that a system will spontaneously change only in the direction from high to low chemical potential. Thus, if a "driving force" $\Delta\mu > 0$ exists, the system is not reversible. This system is better represented by Figure 1b, where the liquid → solid and solid → liquid reactions are distinct and are not microscopically reversible because each direction must take a different path. Because the stable form of a substance will be exclusively the single phase of lowest chemical potential, any phase transition is irreversible, except at the unique T and P conditions of equilibrium. Again, it is important to emphasize that the $\Delta\mu$ of the reaction gives no

https://dx.doi.org/10.1021/acs.jpcc.0c03003
J. Phys. Chem. C 2020, 124, 18724−18740

indication as to the magnitude of the activation barrier which controls the rate of the reaction.

The T and P conditions under which equilibrium exists are defined by eq 9.

$$\frac{dP}{dT} = \frac{\Delta H}{T\Delta V} \tag{9}$$

Because ΔV is very small for a liquid−solid transition, dP/dT is very steep. Thus, the reversible equilibrium condition under normal experimental conditions is essentially a single point. This is in notable contrast to reactions in dilute media (gas−solid, gas−liquid, or dilute solution−crystal transitions) for which ΔV is large and thus dP/dT is relatively shallow such that equilibrium conditions are observed over a substantial range of pressure (concentration) and temperature conditions. Thus, unlike reactions in dilute media, unless working across extreme pressures, an equilibrium constant between solid and liquid is not definable when the system is below or above the T_m.

Furthermore, even for a reversible equilibrium, the transition state theory describes the rates of forward and reverse reactions independently.[14] The relationship between forward and reverse rates defines the thermodynamic equilibrium constant $K = k_f/k_r$, k_f and k_r being the rate constants for the forward and reverse reactions, respectively. Notably, because of the irreversibility of the chemical potential for a first-order phase transition, $k_f = 0$ (e.g., for crystallization) above T_m and $k_r = 0$ (e.g., for melting) below T_m. Thus, descriptions of the rate of crystal growth for a system crystallizing from a supercooled melt cannot be defined by the relative rates of attachment and detachment.

3.2. Independent Particle Assumption. Observations of fast growth within a growth layer and slower propagation of layers for crystal growth from dilute media were explained by the attachment of independent crystal growth units (atoms, ions, and molecules) to crystalline surfaces at specific edge or kink sites.[17,18] Frenkel applied a similar conception to melt crystallization suggesting that a classical activation theory of independent particles transitioning from a liquid to a solid state accounted for the influence of temperature on the rate of crystal growth.[5] With few exceptions,[29] most models of crystal growth still rely on those early conceptions of a binary distinction of growth units existing in either a liquid or crystalline state, with a definable interface with faces, steps, and kinks separating them.[21,28] However, such a binary conception is inconsistent with the actual distinction between liquid and crystalline structure.

The independence of growth units in a melt, or lack thereof, and whether or not an interface exists between a solid and its melt can be visualized by consideration of the 2-D tennis ball models of a "crystal" and "liquid" in Figure 2. The close-packed tennis balls (Figure 2a) provide a model of a simple crystal. In Figure 2b, the frame enclosing the tennis balls was enlarged equivalent to a 15% volume expansion and the tennis balls were agitated to fill the space. A 15% volume expansion is consistent with that observed for the melting of crystalline argon, a system reasonably modeled as hard spheres, but is substantially greater than that observed for most solid/melt systems which exhibit networks or even modest intermolecular interactions; H_2O contracts by 9% between crystal and melt at T_m = 0 °C, whereas between crystal and melt, Al expands by 2% at T_m = 660 °C and SiO_2 expands by 6% at T_m = 1710 °C. In the 15% expanded volume of the Figure 2b model, a few tennis ball "atom−atom" contacts remain the same as in the original "crystal," but no contacts increased by more than 20%. The distribution of pair correlations of the tennis balls for the "crystalline" and "liquid" models is shown in Figure 2c. Notably, if the tennis balls represent Al atoms, given a metallic radius of 1.40 Å and a van der Waals radius (r_{vdW}) of 1.84 Å (shown as blue circles around three tennis-ball atoms), no Al−Al bonds would be fully broken, unless the atom−atom distance increases by greater than 31%, that is, greater than the sum of their r_{vdW}. With Al exhibiting only a 2% volume expansion upon melting, although the long-range ordered lattice structure clearly is disrupted, no short-range Al−Al bonds are broken in the melt! Similarly, the sum of Si and O r_{vdW} is 3.63 Å, which can be compared to the 1.61 Å Si−O bond distance in cristobalite. Thus, a 125% bond expansion is required for atomic separation beyond the sum of their r_{vdW} in order to fully break bonds such that any growth unit could be treated as independent.

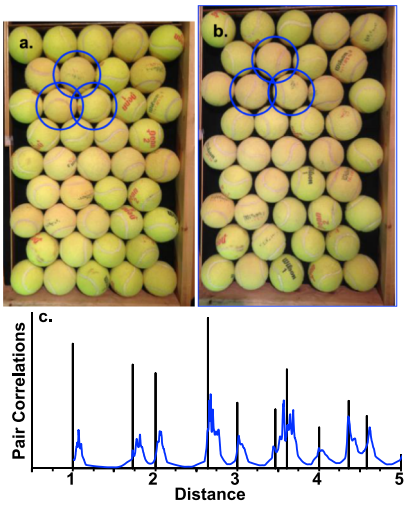

Figure 2. (a) 2-D tennis ball model of a close-packed atomic crystal. (b) 2-D tennis ball model distributed in an area equivalent to a 15% volume expansion. Blue circles represent the relative r_{vdW} if the tennis balls represent Al atoms. (c) Distribution of pair correlations of tennis balls in the "crystalline" frame (black) and in the "liquid" frame (blue, upscaled by 5×).

This tennis ball model does not reveal anything that is not already well known about the structural chemistry of liquids. Although a hard-sphere type material, such as argon, exhibits significant structural rearrangement between crystalline and liquid states,[30] network materials such as SiO_2 or $ZnCl_2$ are well known to remain networks in the liquid state.[31,32] Their short-range order is essentially equivalent between crystalline and liquid phases, and intermediate-range order has been observed out to at least 5 nm. We have even shown that zeolite-type cage structures are maintained in the melt of halozeotypes $A_n[Cu_nZn_{m-n}Cl_{2m}]$.[33] Similarly, melt structures of metal alloys have been shown to exhibit several atomic layers with crystal-like order above crystalline surfaces.[34,35]

Clearly, except for hard-sphere systems such as argon,[30] the difference between crystalline and liquid structure is insufficient for any growth units to be considered independent species in the melt or for there to exist a crystalline interface with distinct step or kink features for additional growth units to attach to. Thus, models for crystal growth should not be based on the binary assumption that growth units are either crystalline or liquid. Instead, models describing crystal growth should consider collective ensembles, rather than independent

https://dx.doi.org/10.1021/acs.jpcc.0c03003
J. Phys. Chem. C 2020, 124, 18724−18740

particles. Such collective ensembles may in part be responsible for what has been described as melt-memory effects, particularly observed for polymers.[36]

3.3. Diffusion/Viscosity Assumption. The assumption that growth units must diffuse through the liquid phase to a crystal growth interface is a direct consequence of the above challenged independent particle assumption. Frenkel described particles in a liquid to be oscillating about a temporary position of equilibrium, which then jump to a new position of equilibrium at a distance δ of atomic dimensions away from the previous one.[5] He described the diffusion constant, D, to be related to this jump distance and an activation energy U' for jumping between consecutive equilibrium positions, eq 10.

$$D = \frac{1}{3}lv = \frac{1}{3}\frac{\delta^2}{\tau_0}\exp\left(\frac{-U'}{k_B T}\right) \tag{10}$$

Applying the Stokes−Einstein relationship, he suggested that the same activation barrier to particle jumping can describe viscosity according to eq 11.

$$\eta = AT\ \exp\left(\frac{U'}{k_B T}\right) \tag{11}$$

where A is a constant. Based on these he stated "Now it seems quite natural to assume that this activation energy is the same or very nearly the same as the activation energy U which is necessary for a transition from an equilibrium position in the liquid to an equilibrium position on the surface of the adjacent crystal of the same substance. Hence, it follows that the linear velocity of crystallization of a given substance considered as a function of temperature at and below the standard crystallization point must be inversely proportional to the viscosity of the latter."[5]

These assumptions remain the fundamental basis of the standard models of crystal growth.[21] However, as schematically represented by the 2-D tennis-ball model of Figure 2, it is clear that atoms/molecules do not need to jump from one site to another for viscous flow or for crystallization. In fact, based on the relative densities of the liquid and solid, most atoms/molecules will not have an adjacent site to jump into. Notably, no voids sufficient to be a "jump site" are created by the 16% volume expansion that would occur by disordering cubic close packing to random close packing. Instead, given the van der Waals overlap between the atoms/molecules even in the liquid state, it is necessary to develop a dynamic model of bonding. To form a crystal from its congruent melt, the atoms/molecules in the melt do not need to diffuse anywhere. Rather, it is necessary for them to organize from a state dominated by short-range order to one exhibiting long-range order, which is clearly a collective, ensemble, rather than independent particle process.

Because dynamic rearrangements of bonding are required for both viscous relaxation and crystal growth, it is not surprising that an experimental correlation, not causation, between viscosity and linear crystal growth rates is observed which was initially reported by Wilson but also recently addressed by several authors.[4,8−10] Notably, a large majority of experimental work demonstrates that the correlation between viscosity and crystal growth rates breaks down for deep supercooling, particularly for fragile liquids. Additionally, it is well known that viscous relaxation is fast with respect to crystal growth.[37−39] Thus, from the perspective of kinetic theory, relaxation may be a fast, initial step, but the fast step cannot be rate determining. The need to introduce additional parameters into classical theories, such as modulating exponents[8] or crossover or decoupling temperatures,[9,10] as well as the invocation of a fast-activated process to describe the slower rate-determining process may well be a signature of the confusion between correlation and causation.

Furthermore, viscosity is a sample-history-dependent phenomenon, the measured viscosity increasing with increased frequency of the probe used to measure it. This is the origin of the well-known time−temperature superposition of viscosity and the glass transition.,[37,40] Notably, no such time−temperature superposition is observed for crystal growth rates. Although fast versus slow quenching of a melt to a crystallization isotherm or up-quenching a glass to a crystallization isotherm exhibits a dramatic impact on nucleation, crystal growth rates are independent of such sample history, dependent only on the temperature of the crystallization isotherm,[41] thus further contra-indicating viscous relaxation exhibiting control over crystal growth rates.

Because of the insufficiency of the above-discussed assumptions of a driving force, the independence of growth particles, and of the correlation between diffusion or viscosity and crystal growth, there is clearly a need for a substantially different model to describe the rate of melt-crystal growth. Any potentially valid model must: (a) describe a first-order irreversible process; (b) describe ensemble, rather than independent particle processes that addresses the cooperativity and configurational entropy of both liquid and crystalline condensed phases, and (c) recognize that crystallization from a congruent melt involves the transformation of intermediate-range order into long-range order, rather than requiring diffusion of matter by attachment to or detachment from an interface.

4. TRANSITION ZONE THEORY OF CRYSTALLIZATION

The rate of crystal growth, which increases with increasing temperature to T_{max} and then slows as the T_m is approached,[3−5] is a thermodynamically irreversible process except at T_m, which is inconsistent with the transition state theory[14] that presumes microscopic reversibility. Nevertheless, crystal growth is an activated process; its rate also being controlled by some activation barrier $\Delta G_c^{\ddagger}$. The formation of the long-range order of a lattice is significantly responsible for the microscopic irreversibility of a crystallization reaction. Thus, an understanding of the irreversible, cooperative, ensemble processes required to form such an ordered lattice likely also provides the key to deciphering details of condensed matter-activated processes.

Undoubtedly, for crystal growth there must be some rearrangement of bonding between melt and crystalline states, and thus an enthalpic contribution to the activation process. However, because short- and intermediate-range interactions are generally quite similar in melt and crystalline phases,[31−33] local enthalpic considerations are not anticipated to dominate the activation landscape. By contrast, reducing the many configurations accessible to a liquid state to the few accessible configurations of a crystal is expected to dominate the activation landscape. Specifically, given the negative sign of the entropy of crystallization, ΔS_c, the entropic contribution to the activation barrier for crystal growth, $-T\Delta S_c^{\ddagger}$, should increase with increasing temperature and thus is likely

https://dx.doi.org/10.1021/acs.jpcc.0c03003
J. Phys. Chem. C 2020, 124, 18724−18740

responsible for the slowed rate of crystal growth between T_{max} and T_m.

Eyring's classical transition state theory describes constant enthalpic and entropic activation parameters corresponding to the transition state over which single particles must pass in the transition from reactant to product, eq 12.

$$k = \frac{k_B T}{h} \exp\left(\frac{-(\Delta H^{\ddagger} - T\Delta S^{\ddagger})}{RT}\right) \tag{12}$$

By contrast, in the condensed phase, the transition between liquid and crystalline states is dependent on the ability to organize an ensemble of particles across a gradient between the short- and long-range order,[34,35] hereafter referred to as the transition zone (TZ), and hence, the description as transition zone theory (TZT).[11] Organization of such an ensemble of particles is dependent on the extent to which those particles cooperate,[13] which is temperature dependent. Thus, activation parameters for condensed matter reactions must be temperature dependent.

Kauzmann recognized that the temperature dependence of the configurational entropy of a crystal, $S_c(T)$, is minimal compared to that of its melt, $S_l(T)$. Thus, if a melt can be sufficiently supercooled, there should exist a temperature T_K at which the configurational entropy of the melt and crystalline phases are equivalent. Based on Boltzmann's description of molar entropy, $S = R\ln(W)$, where R is the gas constant and W is the molar number of microstates or configurations, as $T \to T_K$, $\Delta S_c = R\ln(W_c/W_l) \to 0$.

In the development of TZT, we suggested that the thermodynamic principles of Kauzmann need to be extended to understand the entropic contributions of the activation energy for crystal growth.[11] Applying Boltzmann's description of molar entropy to the activation process for melt crystallization

$$\Delta S_c^{\ddagger} = S^{\ddagger} - S_l = R\ln\left(\frac{W^{\ddagger}}{W_l}\right) \tag{13}$$

where $W^{\ddagger}$ is the molar number of configurations in the TZ and W_l is the molar number of configurations in the supercooled liquid. Thus, the entropic probability for an ensemble to rearrange into a specific TZ configuration is directly proportional to the number of the microstates of the TZ compared to that of the reactant phase, as described by eq 14.

$$\exp\left(\frac{\Delta S_c^{\ddagger}}{R}\right) = \frac{W^{\ddagger}}{W_l} \tag{14}$$

It is reasonable to assume that at T_K, where there are an equivalent small number of configurations accessible to the melt and crystal, there should be a similarly small number of transition configurations that could transform the melt to a crystal. Thus, as $T \to T_K$, $W^{\ddagger}/W_l \to 1$ and $\Delta S_c^{\ddagger} \to 0$. For most systems, crystallization or glass formation will occur before T_K is achieved; nevertheless, $\Delta S_c^{\ddagger}$ will become less negative with deeper supercooling. At higher temperatures, although the number configurations accessible to transform the melt to a crystal remain few, the number of configurations accessible to the melt will substantially increase such that as $T \to T_m$, $W^{\ddagger}/W_l \to$ few/many $\to 0$ and thus $\Delta S_c^{\ddagger} \to -\infty$. Above T_m, the probability of achieving a crystallization TZ is not defined.

These boundary conditions for $\Delta S_c^{\ddagger}(T)$ can be described by eq 15

$$\Delta S_c^{\ddagger}(T) = \Delta S_c^{*}\left(\frac{T - T_K}{T_m - T}\right)^{z_c} \tag{15}$$

where ΔS_c^{*} is an intrinsic entropic activation parameter, and z_c modulates the temperature dependence of the entropy of activation. Although first presented as an empirical parameter,[11] based on the data presented below, we now suggest that z_c is correlated to $-R/\Delta S_c^{*}$, which, based on Boltzmann's relationship, suggests that it is a reflection of the ratio of configurations of the intrinsic growth units in the TZ and supercooled melt phases. Notably, if there is no cooperativity in a system (i.e., a gas or dilute solution), z_c should go to zero, such that the Eyring-transition-state condition for independent particles, and thus a temperature-independent activation entropy dependence, would be observed.

Although the short- and intermediate-range order (local bonding) is very similar between melt and crystalline phases and limits the local enthalpic influence on activation, there is a direct correlation between any enthalpic barriers and the extents of cooperativity of the system. Herein, there must be some intrinsic interparticle enthalpic activation parameter, ΔH_c^{*}, indicative of the bond reconstruction required for the transformation, which must be scaled to the number of units that must interact as a cooperative ensemble. If a system could be supercooled to T_K, the entire system would need to cooperate for any transformation. By contrast, at higher temperatures, the cooperative regions will be diminished such that in the high-temperature limit only the intrinsic interparticle term needs be considered. Unlike the entropy of activation, the temperature dependence of the enthalpy of activation is not impacted by T_m because as modeled above in Figure 2, bonds are not broken at T_m. We thus adapted a classic Adam–Gibbs expression for cooperativity[13] to express the temperature-dependent enthalpic activation, eq 16.

$$\Delta H_c^{\ddagger}(T) = \Delta H_c^{*}\left(\frac{T}{T - T_K}\right) \tag{16}$$

Notably, at high temperature, where $T \gg T_K$ or if $T_K = 0$, the temperature-dependent term goes to 1 such that the Eyring-transition-state condition of a constant enthalpy of activation is observed.

In addition to the temperature-dependent descriptions of the enthalpic and entropic activation parameters, to adapt the concepts of Eyring's transition state theory (eq 12) to condensed matter reactions, it is also necessary to address the attempt frequency prefactor, which for crystal growth must have units of distance per time. In the transition state theory, the prefactor is the product of the number of vibrations in the transition state ($k_BT/h\nu$) and the frequency of those vibrations, ν. By contrast, for crystallization, as described by our TZT, the attempt frequency prefactor is the product of the lattice vibrational modes that lead to the formation of the crystalline phase, ($k_BT/h\nu$) and the velocity of the transition zone, $\lambda\nu$, where λ is a characteristic wavelength of vibrations that lead to crystal growth. Using the lattice harmonic oscillator approximation, we postulate that λ corresponds to the first Brillion zone of the allowed lattice vibrations.[42] For a cubic system, $\lambda = 2a$. For analysis of noncubic systems, we approximate this as $\lambda \approx 2 \times V^{1/3}$, though clearly growth-face specific analysis should be possible.

https://dx.doi.org/10.1021/acs.jpcc.0c03003
J. Phys. Chem. C 2020, 124, 18724–18740

Combining this prefactor with the temperature-dependent enthalpic and entropic probabilities yields the TZT_c expression, eq 17.[11]

$$\nu_{pb} = \lambda\frac{k_B T}{h}\exp\left(\frac{-\Delta H_c^*}{R(T - T_K)}\right)\exp\left(\frac{\Delta S_c^*}{R}\left(\frac{(T - T_K)}{(T_m - T)}\right)^{z_c}\right) \quad (17)$$

Importantly, λ and T_m can be directly and independently measured, and T_K can be independently measured by extrapolation of the respective temperature-dependent heat capacity of the melt and crystalline phases.[43] Thus, this TZT_c expression requires only three fitting parameters. (If not independently measured, T_K also may need to be fit.) ΔH_c^* and ΔS_c^* describe the intrinsic enthalpic and entropic components of the activation free energy. The parameter z_c, which modulates the temperature dependence of the entropy of activation, reflects the cooperativity of the system.

Before considering the application of TZT_c to actual systems, it is useful to visualize the temperature-dependent behavior of the enthalpic and entropic activation parameters, as well as the impact of the cooperativity parameter z_c. In Figure 3a, the temperature-dependent entropy of activation, $\Delta S_c^{\ddagger}(T)$,

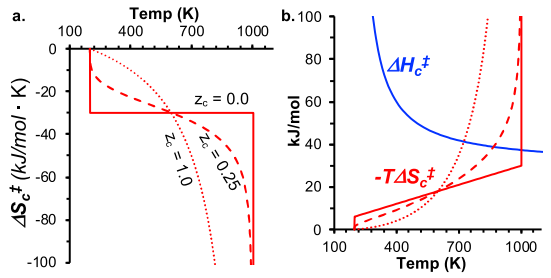

Figure 3. Visualization of components of TZT_c and their impact by variation in the z_c parameter: $z_c = 0$ (solid), = 0.25 (dashed), and = 1.0 (dotted). (a) Temperature dependence of $\Delta S_c^{\ddagger}$ and (b) temperature dependence of $\Delta H_c^{\ddagger}$ (blue line) and $-T\Delta S_c^{\ddagger}$ as a function of z_c (red lines). Data are calculated with an arbitrary set of parameters: T_m = 1000 K, T_K = 200 K, ΔH_c^* = 30 kJ/mol, and ΔS_c^* = −30 J/mol·K.

is plotted using an arbitrary set of parameters for three different values of z_c. In Figure 3b, the temperature-dependent enthalpic, $\Delta H_c^{\ddagger}(T)$, and entropic energy, $-T\Delta S_c^{\ddagger}(T)$, terms are plotted, again for three distinct values of z_c. The temperature-dependent free energy of activation, $\Delta G_c^{\ddagger}(T)$, is the sum of these two functions. When $z_c = 0$, the $\Delta S_c^{\ddagger}(T)$ is constant over the entire range from T_K to T_m. This results in a linear increase in the $-T\Delta S_c^{\ddagger}$ contribution to the free energy of activation with increasing temperature. Larger values of z_c, however, reflect the temperature-dependent effects of cooperativity on $\Delta S_c^{\ddagger}$. An inverse energetic impact is observed for the enthalpy of activation, increasing to infinity at low temperature and decreasing to the constant value of ΔH_c^* at high temperature where the temperature-dependent term $T/(T - T_K) \rightarrow 1$. Importantly, for a system with $z_c = 0$, that is, exhibiting essentially no cooperativity, and at high temperature, the TZT_c expression, eq 17, collapses to the Eyring transition state theory expression, eq 12, with the prefactor multiplied by λ.

5. COMPARING TZT_C TO STANDARD MODELS

5.1. Contrasting Results. In our previous reports, we demonstrated that the TZT_c accurately describes the temperature-dependent growth rates of diverse systems ranging from the strong SiO_2 to the fragile *ortho*-terphenyl (OTP).[11,36,40,44] However, in none of those reports was the TZT_c model directly compared to fits of data to standard models. Although it is never possible to prove a mechanistic model correct, some degree of validation is afforded to models that best fit experimental data with the fewest number of fitting parameters and for which the parameters have chemical/physical meaning, as opposed to empirical fitting parameters. Herein, TZT_c does not rely on the incorrect assumptions of a driving force (microscopic reversibility), isolated particles (discrete interfaces), or the diffusion of particles (or its correlation to viscous relaxation) to describe crystal growth rates. Rather, TZT_c only relies on the existence of enthalpic and entropic barriers to organization of ensembles of growth units into the transition zone, for which their temperature dependence is governed by the cooperativity of the growth units in the melt. Of the three fitting parameters in TZT_c (ΔH_c^*, ΔS_c^*, and z_c), only z_c is a semi-empirical parameter, though as will be demonstrated below, this parameter appears to be a function of the ratio of the number of configurations of the intrinsic growth units in the TZ and melt.

To accomplish the comparison of TZT_c to standard models of crystal growth, we here evaluate the same crystallizing systems that were evaluated by Nascimento and Zanotto[15] and Ediger et al.[8] in their attempts to describe the decoupling of viscous relaxation and crystal growth rates for which normal, screw, and 2-D standard models were applied. Figure 4 provides analogous plots to those presented in ref 15, along with data for three additional materials, for which reported experimental growth-rate data is compared to reported fits to standard models, along with plots of the fit to our TZT_c model. Literature parameters were utilized to reproduce the reported standard model fits. TZT_c parameters for these and other materials we have evaluated, in addition to references to the experimental data, are given in Table 1.

In each case, TZT_c yields an equivalent to superior fit to the experimental data than fits to standard models, as clearly seen in the plots of the residuals between experimental data and the respective fits to models given in Figure 4. More importantly, there is no decoupling between the TZT_c model and the experimental data at deep undercooling as frequently observed with the standard models.

Improvement to normal model fits was achieved by Ediger et al. by correcting for the apparent decoupling of viscosity, η, from the reduced growth rate, u_{kin}, with the introduction of the parameter ξ, to reflect an apparent power-law dependence between them; $u_{kin} \propto \eta^{\xi}$.[8] They concluded that the exponent ξ is correlated with the fragility, m, according to the empirical relationship $\xi \approx 1.1 - 0.005m$ for both organic and inorganic materials, albeit with a distinct relationship required for Li^+-containing materials.[8] This modification to the standard model reduces residuals between experiential and modeled data. That said, based on their reported results, systems are described with $\xi = 0.79 \pm 0.01$ for $44 < m < 89$ and with $0.6 < \xi < 0.84$ for $m = 80 \pm 4$, clearly limiting the predictive utility of any apparent correlation.

Schmelzer et al.[9] and Cassar et al.[10] proposed a different modification by which a decoupling temperature, T_D, is introduced to correct for the apparent decoupling of viscosity from the standard model. The best decoupling temperature models fit the experimental growth rate data for diopside equivalently to the fit with our TZT_c model. However,

https://dx.doi.org/10.1021/acs.jpcc.0c03003
J. Phys. Chem. C 2020, 124, 18724−18740

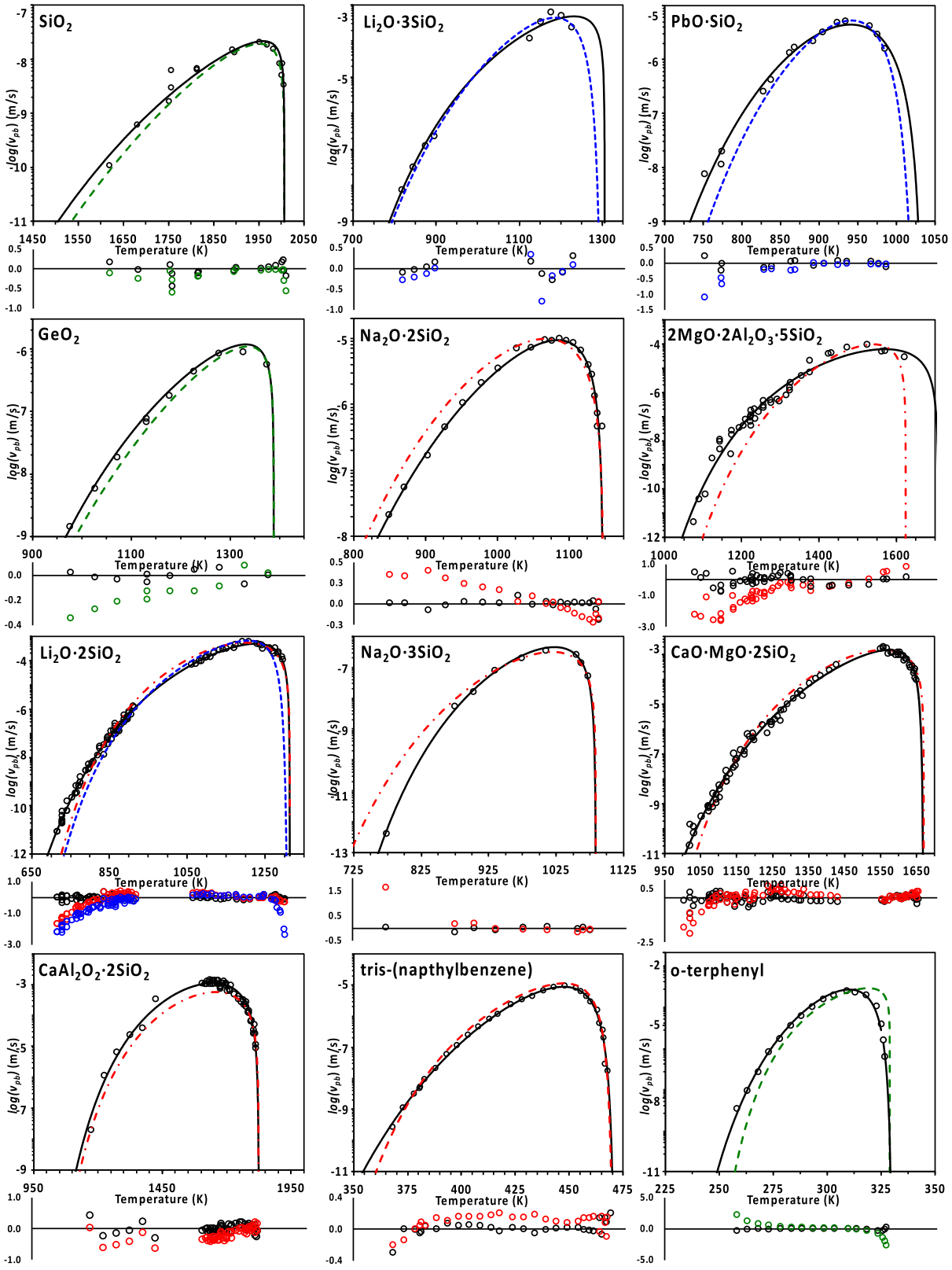

Figure 4. Experimental crystal growth rate data (open circles), fit to TZT_c (solid black line), and compared to the literature reports of standard models (normal (green dashed), screw (red dashed) and 2D (blue dashed)). Below each figure is a plot of the respective residuals between the TZT_c calculated values (black circles) and the values calculated by the respective standard models. (Note, for OTP literature standard model parameters have not been found, with reports suggesting that it is poorly fit. The curve shown is our best fit to the normal model using reported VFT viscosity parameters.)

independent physical evidence does not support the decoupling of diffusion and viscosity; the decoupling instead likely is an artifact of the VFT equation's incomplete modeling of viscous relaxation.[27] Furthermore, the TZT_c model employs

https://dx.doi.org/10.1021/acs.jpcc.0c03003
J. Phys. Chem. C 2020, 124, 18724−18740

Table 1. TZT_c Parameters

Compound	T_m (K)	T_K (K)	$\sqrt[3]{V}$ (Å^3)	ΔH_c^* (kJ/mol)	ΔS_c^* (J/mol·K)	z_c	Figure symbol	References
SiO_2[a]	2007	484	7.149	250	-70.7	0.062		45, 46
GeO_2-(series-1[b])	1388	294	5.006	139	-64.2	0.089		47
$Li_2O{\cdot}2SiO_2$	1313	337	8.432	109	-27.5	0.239		15, 48-56
$Li_2O{\cdot}3SiO_2$	1306	365	10.171	105	-28.6	0.239		57, 58
$Na_2O{\cdot}2SiO_2$	1147	348	8.909	106	-35.4	0.205		59
$Na_2O{\cdot}3SiO_2$	1084	529	9.200	68.4	-62.1	0.176		60
$PbO{\cdot}SiO_2$	1037	442	10.157	68.5	-43.2	0.313		15, 61
$CaO{\cdot}MgO{\cdot}2SiO_2$ (diopside)[c]	1670	534	7.965	148	-5.49	0.578		10, 15, 62-65
$2MgO{\cdot}2Al_2O_3{\cdot}5SiO_2$ (cordierite)[d]	1708	743	12.043	85.0	-67.0	0.169		62
$CaAl_2Si_2O_8$ (anorthite)	1825	815	11.025	68.6	-65.6	0.177		10, 66
$NaPO_3$	898	128	10.104	79.9	-49.2	0.207		67
$LiPO_3$	926	350	10.473	39.2	-92.1	0.127		68
CZX-1 – d_0	446	150	10.589	37.7	-8.0	0.584		41
CZX-1 – d_1	448	157	10.559	38.7	-1.6	1.13		41
CZX-1 – d_9	447	203	10.570	26.8	-16.0	0.532		41
CZX-1 – d_{10}	446	213	10.563	27.1	-11.0	0.683		41
$ZnCl_2{\cdot}3H_2O$	280	222	8.399	0.51	-142	0.078		44
Tris-(napthyl)benzene)	331	209	13.487	43.7	-2.28	0.881		69
OTP	331	200	10.950	14.7	-10.8	0.662		70
salol I (stable)	315	167	12.801	16.3	-13.5	0.483		71
salol II (metastable)	302	183	10.170	10.8	-51.9	0.159		71
α-phenyl o-cresol	324.5	181	12.662	9.79	-69.2	0.182		72
ROY Y	383	237	8.427	5.07	-107	0.089		73
ROY R	379	220	10.596	7.09	-104	0.072		73
α-indomethacin	426	256	13.576	16.2	-67.3	0.128		74
γ-indomethacin	433	230	9.539	26.2	-26.2	0.356		74
δ-indomethacin	400	259	11.558	15.0	-69.7	0.115		74
Sorbitol	368	196	13.450	21.1	-39.6	0.275		75
glycerol	291	134	7.597	14.4	-55.7	0.197		16

[a]Both Wagstaff data sets (refs 44 and 45) were used for the analysis reported here to mirror the standard model analysis in ref 15. Our previous TZT_c analysis of SiO_2 crystallization (ref 11) did not utilize data from ref 45 because that report indicates significant oxygen deficiency of the system. [b]For comparison to the data analyzed in ref 15, growth-rate data from ref 46 series-1 was used. That was the most oxygen deficient series measured. Data for the least oxygen deficient series-4 suggests higher enthalpic and lower entropic parameters. [c]TZT_c parameters are based on the fit to all data as opposed to the more limited set of data for fitting in ref 10. [d]The reported fit to the normal model utilized T_m = 1623, the lower bound estimated for the metastable μ-polymorph.[15] The TZT_c fit to the data uses T_m = 1708 K of the stable α-polymorph.

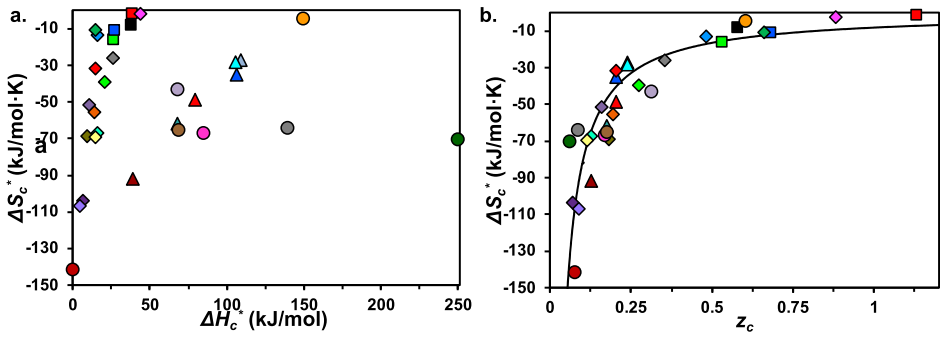

Figure 5. (a) Correlation between ΔH_c^* and ΔS_c^*. (b) Correlation between ΔS_c^* and z_c. The solid line in b corresponds to the correlation $\Delta S_c^* = -R/z_c$. The shapes and colors of symbols identify the compounds as described in Table 1.

https://dx.doi.org/10.1021/acs.jpcc.0c03003
J. Phys. Chem. C 2020, 124, 18724−18740

fewer fitting parameters and does not require terms that incorporate the incorrect assumptions of viscous relaxation and a driving force to describe the crystal growth.

5.2. Chemical/Physical Mechanistic Insight from TZT_c. With a single model that effectively describes diverse crystallizing systems, from strong inorganic networks to fragile organic molecular systems, the three parameters extracted from TZT_c can, for the first time, afford an ability to compare and contrast chemical and/or physical factors that influence crystallization reactions. The same is not possible using the standard models which use distinct sets of parameters for normal, screw, and 2-D standard models. To begin evaluating such chemical/physical factors across diverse crystallizing systems, it is useful to consider the ΔH_c^* versus ΔS_c^* and z_c versus ΔS_c^* correlation plots given in Figure 5, for which all data is given in Table 1.

We previously observed significant correlations between the ΔH_c^* and ΔS_c^* activation parameters and chemical/physical attributes of the crystallizing materials. For example, SiO_2 (dark green circle in Figure 5a) exhibits large enthalpic and large negative entropic activation parameters, suggesting that significant "bond energy" is required to form the transition zone, and the transition zone is significantly more ordered than the melt structure. The high enthalpic barrier is consistent with the strong Si−O network bonding, and the large negative entropic activation parameter is consistent with experimental measurements which demonstrate a proliferating number of smaller $(SiO)_n$ rings in the liquid, as opposed to the $n = 6$ rings in cristobalite.[76] By contrast, the fragile OTP (green diamond in Figure 5a) exhibits very small ΔH_c^* and ΔS_c^* activation parameters, suggesting that limited rearrangement of only weak interactions is required to achieve its TZ. The small enthalpic term is consistent with weak π-stacking intermolecular forces, and the small entropic activation parameter is consistent with previous observations that the phenyl rings of OTP form interlocking clusters of molecules in the melt, thus requiring minimal structural organization to achieve a crystallization TZ.[77,78] The fragile tris-(naphthyl)benzene (pink diamond in Figure 5a) exhibits an even smaller entropic activation parameter consistent with greater order in the liquid state due to more extensive π-stacking of the larger naphthyl rings, but its enhanced π-stacking increases the enthalpic barrier required to rearrange molecules to construct long-range crystalline order from the liquid. Interestingly, crystallization of the ionic-liquid molten-hydrate $[Zn(OH_2)_6][ZnCl_4]$ (maroon circle Figure 5) exhibits the smallest enthalpic and most negative entropic activation parameter of any of the inorganic materials we have evaluated. The small ΔH_c^* is consistent with minimal bond energy requirements to reorient the hydrogen bonding of the molecular ions. However, the large negative ΔS_c^* came as a surprise given the equivalent CsCl-type packing of molecular ions in both melt and crystalline states.[79] Here, the entropic TZT_c parameters offer new chemical insight, suggesting that the highly mobile water protons in the liquid must be ordered for crystallization to occur.[43]

Additional materials measured since our initial report, and literature examples evaluated for this article, provide further chemical/physical insight into the z_c parameter. All these materials exhibit a common apparent correlation between the ΔS_c^* and z_c parameters that, with both parameters approaching asymptotes, was originally modeled using a hyperbolic cosecant function $\Delta S_c^* = -3csch(z_c/3)$.[11] Upon further consideration, we find that this correlation is equivalently modeled by the much simpler function $\Delta S_c^* = -R/z_c$; the correlation line is shown in Figure 5b. Based on Boltzmann's relationship, this correlation suggests that $1/z_c = \ln(W_{liq}/W_c^{\ddagger})$ of the intrinsic growth units (i.e., the unit part of the system that may cooperate with other units as a function of temperature). Systems with the least difference between W_{liq} and $W_c^{\ddagger}$ of their intrinsic growth units, that is, with small negative ΔS_c^*, also might be expected to exhibit supercooled-melt structures that are most similar to their crystalline structure. Having the most order to lose with diminished cooperativity at higher temperature, such systems are expected to exhibit the greatest temperature dependence of $\Delta S_c^{\ddagger}$, that is, largest z_c. By contrast, systems with a large difference between W_{liq} and $W_c^{\ddagger}$ of their intrinsic growth units, that is, large negative ΔS_c^*, are anticipated to require substantial structural reorganization to achieve a TZ across the entire temperature range, whether large or small cooperative ensembles, thus resulting in the least temperature dependence for $\Delta S_c^{\ddagger}$, that is, smallest z_c (see Figure 5b). Although the ΔS_c^* and z_c parameters clearly appear to be correlated, explicit use of this correlation to reframe eq 15 with fewer variables does not result in as good of a fit to experimental growth rate data, suggesting that these two parameters in fact address independent factors of the entropy of activation and cooperativity.

The impact of the comparative melt and crystal structures on the relative temperature dependence of the entropic activation is evident in the ΔS_c^* and z_c parameters for diopside as compared to other alkali or alkaline earth silicates, for which diopside appears to be an entropic outlier. The ΔH_c^* parameter of diopside is the largest of all alkali or alkaline earth cation-substituted silicates evaluated here, consistent with an activation enthalpy required to rearrange strong M−O/Si−O bonding with the high charge density M = Mg^{2+} and Ca^{2+} cations. By contrast, diopside exhibits $\Delta S_c^* = -5.49$ J/mol·K, which is about one-fifth of that of the next closest silicate, and the greatest temperature dependence of the entropy of activation with $z_c = 0.6$, which is more than twice that of the next closest silicate. This is consistent with diopside exhibiting the most condensed crystalline structure of this set of silicates, and a less than a 3% change in density between liquid and crystalline phases.[80] Interestingly, diopside also is considered the most fragile of the set of inorganic oxides examined here,[8] as defined by the Angell fragility scale (i.e., temperature dependence of the viscosity in the vicinity of the glass transition).[81] The strong interactions resulting from the high charge density of the Mg^{2+} and Ca^{2+} cations in diopside seem inconsistent with a high fragility but are consistent with diopside's large ΔH_c^* parameter. By contrast, the small negative ΔS_c^* and relatively large z_c parameters, a consequence of similar melt and crystalline structures, result in the greatest temperature dependence of the activation parameters and are the likely origin of the reported apparent relationship between its growth rate and high fragility value.[8]

The utility of this common set of activation parameters (ΔH_c^*, ΔS_c^*, and z_c) to assess diverse chemical/physical systems provides to crystallization mechanistic investigation a Hammett plot[82]-like tool to evaluate the influence of functional groups or specific structures/bonding on the chemical reactivity.

5.2.1. Molecular Functional-Group Control. Consider, for example the family of ortho-substituted benzene molecules

https://dx.doi.org/10.1021/acs.jpcc.0c03003
J. Phys. Chem. C 2020, 124, 18724−18740

{OTP, two polymorphs of salol, α-phenyl *o*-cresol, and two polymorphs of 5-methyl-2-[(2-nitrophenyl)amino]-3-thiophenecarbonitrile (ROY)} for which crystal growth rate data is reported in the literature. An approximately linear correlation between their ΔH_c^* and ΔS_c^* parameters is observed, and is highlighted in Figure 6 (an expanded and selected view of Figure 5).

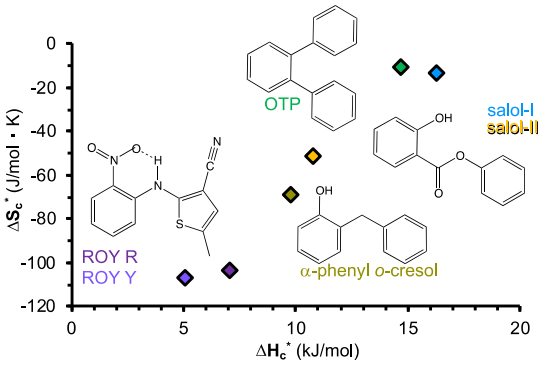

Figure 6. Correlation between ΔH_c^* and ΔS_c^* for a series of ortho-substituted benzene molecules.

All these molecular systems are expected to exhibit only weak intermolecular interactions: a combination of hydrogen-bonding and π-stacking. Initially unexpected, the addition of strong hydroxyl and amino hydrogen-bond donors and carbonyl, nitro, and carbonitrile hydrogen-bond acceptor functional groups does not correlate with an increased enthalpic activation parameter. If anything, there is an inverse correlation between the potential for hydrogen bonding and ΔH_c^*. However, decreasing the degrees of freedom for intramolecular reorientation seems to increase the enthalpic barrier. Notably, while forming weaker intermolecular enthalpic interactions than regular hydrogen-bonding, the π-stacking ability of aromatic functional groups can have a substantial structure directing impact, even in the liquid state.[76,77,83] The structure directing impact of more rigid planar functional groups results in materials that exhibit a greater extent of cooperativity at a higher temperature. This results in higher enthalpic and lower entropic activation parameters and correspondingly greater temperature dependence to its $\Delta S_c^{\ddagger}$, reflected in the larger z_c parameter. Linking a phenyl group to the benzene core through a conformationally flexible methylene bridge in α-phenyl *o*-cresol significantly reduces the extent of functional-group-determined structure direction. With its much weaker cooperativity, a decreased ΔH_c^*, significantly more negative ΔS_c^*, and corresponding smaller z_c parameters are observed.

Interestingly, the two salol polymorphs exhibit activation parameters that approximately mirror those of OTP and α-phenyl *o*-cresol, respectively; salol-I analogous to the more rigid OTP and salol-II analogous to the more conformationally flexible α-phenyl *o*-cresol. Notably, the crystal structure of the thermodynamically stable salol-I phase[84] exhibits strong face-to-face π-stacking of the phenol and ester units forming molecular dimers, which are further networked by hydroxyl-to-carbonyl hydrogen bonding. Salol-I exhibits a higher melting point and is reported to crystallize from melts close to the melting point (T_m = 315 K). These physical characteristics are consistent with the TZT_c parameters which suggest that crystalline salol-I grows from a more cooperative melt (i.e., larger ΔH_c^*, less negative ΔS_c^*, and larger z_c). By contrast, the crystal structure of the metastable salol-II exhibits notably less intermolecular cooperativity with more limited edge-to-face π-stacking and only hydroxyl-to-hydroxyl hydrogen bonding.[85] Salol-II's melting temperature is 13° lower than salol-I and is reported to grow from the melt when quenched from a higher temperature (373 K). Correspondingly, the TZT_c parameters for salol-II exhibit lower cooperativity (i.e., smaller ΔH_c^*, more negative ΔS_c^*, and smaller z_c).

The nitro and amino-bridge functional groups of the ROY ortho-substituted benzene exhibit even greater conformational flexibility and are likely the cause of the further diminished enthalpic barrier but more negative entropic crystallization barrier and corresponding less temperature dependence to its $\Delta S_c^{\ddagger}$, reflected in the small z_c parameter. The high degree of conformational flexibility combined with multiple functional groups capable of distinct patterns of intermolecular interactions such as hydrogen-bonding and π-stacking may be responsible for the observation of multiple ROY polymorphs.[86]

The crystal growth rates of the more complex and polymorphic indomethacin exhibit a trend consistent with that observed for the ortho-substituted benzene molecules (Figure 5). The indole core provides a broader planar molecular backbone than does benzene. The organic acid groups result in intermolecular hydrogen bonding. However, the ether, methylene, and amide linking groups introduce substantial intramolecular conformational flexibility. Notably the crystal structure of the stable γ-phase, which directly crystallizes from the melt, exhibits hydrogen-bonded molecular dimers linked by the organic acid functional groups, as well as face-to-face π-stacking of the indole cores.[87] The cooperativity of the crystalline structure which likely persists in the melt is consistent with the observation of the relatively larger ΔH_c^*, less negative ΔS_c^*, and larger z_c activation parameters, similar to those of OTP and the stable salol-I. By contrast, the metastable α- and δ-phases only grow from seeded melts, initially grown from alcohol solutions, and exhibit melting points 7 and 33° below that of the γ-phase, respectively.[73,88] The crystal structure of the α-phase also exhibits acid-hydrogen bonded dimers but substantially less intermolecular π-stacking is observed than is observed for the γ-phase. No crystal structure is reported for the δ phase. The less cooperative structure of the α- and δ-phases, along with the likely substantial difference between melt and crystal structures given their growth from the melt requires seeding, is consistent with the observed smaller ΔH_c^*, more negative ΔS_c^*, and smaller z_c activation parameters, which are similar to the more conformationally flexible α-phenyl *o*-cresol and metastable salol-II.

Although we have identified fewer reports of crystal growth-rate data for polyalcohols, the crystal growth rates of sorbitol and glycerol exhibit analogous trends with respect to conformational flexibility controlling crystal growth rates. Glycerol, a six-carbon chain with six hydroxyl functional groups, has greater H-bonding capability and greater conformational flexibility than sorbitol's three carbon-chain with three hydroxyl functional groups. As seen in Figure 5a, however, glycerol (orange diamond) exhibits smaller enthalpic but greater entropic activation parameters than does sorbitol (green diamond). These data are consistent with the observation that molecular conformational flexibility has a

https://dx.doi.org/10.1021/acs.jpcc.0c03003
J. Phys. Chem. C 2020, 124, 18724−18740

dominant impact on a system's cooperativity and thus significantly controls the barrier to its crystal growth.

5.2.2. Controlling the Formation of Inorganic Networks. Inorganic networks do not offer the same level of parameter control as can be achieved by manipulating functional groups of organic molecules. Nevertheless, any influence templating ions might have on crystal growth rates of inorganic frameworks could be revealed as systematic variations of activation parameters. Furthermore, it is expected that common crystal structure types or common crystallizing processes should exhibit consistent sets of activation parameters.

Exploiting the mechanistic detail accessible with TZT_c, a kinetic isotope effect investigation was conducted to probe how the interaction between a templating cation and a metal halide framework might impact the kinetics of crystal growth.[40] Measurements of the temperature-dependent crystal growth rates for the sodalite-type halozeotype CZX-1, $[HNMe_3]$-$[CuZn_5Cl_{12}]$, were made with d_0, d_1, d_9, and d_{10} isotopic substitution of the $[(H/D)N(C(H/D)_3)_3]^+$ templating cation. As evident from the expanded ΔH_c^* versus ΔS_c^* plot in Figure 7, comparison of the d_0 and d_9 isotopomers to the d_1 and d_{10}

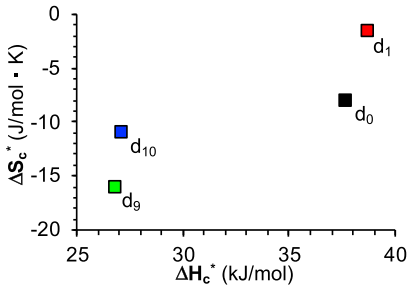

Figure 7. Correlation between ΔH_c^* and ΔS_c^* for the isotope effect on the crystallization of CZX-1, $[(H/D)N(C(H/D)_3)_3][CuZn_5Cl_{12}]$.

isotopomers, respectively, reveals that stronger deuterium bonding between the alkylammonium cation and the framework chlorides requires a slightly higher enthalpic barrier for crystallization, whereas the slightly stronger ND-framework interaction increases the structural organization in the melt such that there is a lower entropic barrier (less negative ΔS_c^*) to crystallization. By contrast, comparison of the d_0 and d_1 isotopomers to the d_9 and d_{10} isotopomers, respectively, reveals that the inertial reorientation of the template exhibits a greater impact on the crystallization barrier, with the heavier isotopomer exhibiting lower and more condensed vibrational and rotational energy levels, as well as more accessible microstates.

The $A_2O{\cdot}nSiO_2$ (A = Li or Na and n = 2 or 3) systems also provide an important series with which to understand contrasting crystal growth-rate models and their underlying chemistry. In their crystalline phases, both Li compounds and the (Na n = 2) material exhibit a common structure-type with layers of alkali oxides separating two or three silica layers.[89−91] The (Na n = 3) phase adopts a distinctly different 3-D networked structure.[92] As evaluated in the Nascimento work, the crystal growth rates of the three structurally homologous phases are described by blended 2-D + screw (Li n = 2), 2-D (Li n = 3), and screw (Na n = 2) growth models.[15] The distinct (Na n = 3) phase is suggested to grow by the screw model. However, there is nothing chemical or physical about the three structurally homologous phases that gives indication as to a reason for them to be described by distinct growth models. By contrast, the TZT_c fits to the growth data demonstrate that all three structurally homologous phases exhibit very similar values of ΔH_c^*, ΔS_c^*, and z_c, consistent with a common path for the melt → crystal transformation. The minor difference between the lithium and sodium disilicates, for which the sodium species exhibit a slightly smaller enthalpic and slightly more negative entropic activation parameters, is consistent with the lower charge density of the Na^+ ion as compared to Li^+. By contrast, the (Na n = 3) phase exhibits a substantially reduced ΔH_c^*, more negative ΔS_c^*, and a decreased z_c parameter (see Figure 5a and Table 1). It is highly unlikely that the strength of Na−O and Si−O bonding changed between the (Na n = 2) and (Na n = 3) phases. However, the significant changes in the activation parameters for the (Na n = 3) phase suggest that greater reorganization of the structure of the melt is required to achieve the TZ for its distinct crystal structure. The TZT_c activation parameters further suggest that the (Na n = 3) system exhibits reduced cooperativity, which potentially contributes to its more isotropic crystalline structure.

Crystallization of the so-called "anionic chain glasses" $LiPO_3$ and $NaPO_3$ are also more effectively explained by TZT_c than by standard models. Previously, it was noted that at large undercoolings, standard models "cannot account for the drastic difference existing between the activation energies for crystal growth and viscous relaxation" of these materials.[67] Similarly, Ediger et al. suggested that a distinct ξ versus m correlation is necessary to describe the $u_{kin} \propto \eta^{\xi}$ relationship for Li^+-containing materials including $LiPO_3$.[8] By contrast, TZT_c accurately describes the temperature dependence of both Li and Na phosphates over the entire measured temperature ranges.[66,67] The TZT_c activation parameters for $NaPO_3$ fall intermediate on a line between those of the lamellar $Na_2O{\cdot}2SiO_2$ and the 3-D $Na_2O{\cdot}3SiO_2$ materials (Figure 5), whereas $LiPO_3$ exhibits the smallest enthalpic and most negative entropic parameters, and corresponding smallest z_c temperature dependence, of any of the inorganic oxides examined. The vitreous, and presumably melt, phases of these phosphates are reported to consist of phosphate chain anions mixed with cyclic polyphosphate anions, which must transform into crystalline structures with only chain or ring structures.[67] (Several polymorphs of both phosphates with chain or ring structures are known, but the polymorph of the crystallizing phases in the reported crystal growth-rate studies are not reported). Such ring/chain reorganization between melt and crystal is also argued to be the cause of the large negative ΔS_c^* parameter for SiO_2.[11] However, uniquely, $LiPO_3$ also exhibits the greatest ionic conductivity of all materials examined here.[93] Thus, we suggest that in addition to ring/chain reorganization required for crystallization, ordering the mobile Li^+ cations into the crystal lattice is significantly responsible for the largest entropic activation barrier for these inorganic oxides (−92 J/mol·K), consistent with the proposed impact of proton mobility on the crystallization of $[Zn(OH_2)_6][ZnCl_4]$.[43]

As highlighted in the above examples, the TZT_c model not only provides equivalent to superior fitting of temperature-dependent crystal growth rate data than fits to standard models, but the activation parameters extracted from the model are consistent with chemical/physical characteristics of the crystallizing species. For the first time, this single model describes diverse crystallizing systems providing the ability to

https://dx.doi.org/10.1021/acs.jpcc.0c03003
J. Phys. Chem. C 2020, 124, 18724−18740

systematically address geometric and functional group effects on crystal growth rates.

6. RE-EVALUATING THE APPARENT CORRELATION BETWEEN VISCOSITY AND CRYSTAL GROWTH RATES

Finally, it is useful to address how the underlying concepts of the temperature-dependent cooperativity in the TZT_c model reveal why there is an apparent decoupling of crystal growth rates and viscous relaxation. As described above, slowed material diffusion commensurate with increased viscosity was suggested to account for decreased crystal growth rates with deep undercooling, that is, below T_{max}. However, as discussed in Section 3.3, viscous relaxation cannot be rate controlling for crystallization because it is generally the faster process and further because viscous relaxation is frequency dependent and crystal growth rates are not. Nevertheless, because crystallization and viscous relaxation are both condensed matter processes that can occur in the same material under equivalent conditions, common configurational and bonding considerations likely control both processes.

As described in our initial report of TZT, the processes of crystallization and viscous relaxation significantly differ in how the temperature dependence of cooperativity impacts each.[11] Application of eq 13 to the process of viscous relaxation demonstrates that the entropy of activation for relaxation, $\Delta S^{\ddagger}_{rlx}(T)$, is determined by the ratio of number of configurations accessible to the transition zone for relaxation to the number of accessible configurations of the quenched nonergodic liquid, $W^{\ddagger}_{rlx}/W_{nonerg\ l}$. If a system could be quenched to T_K because of the complete cooperativity of the relaxed liquid, there can only be a small number of accessible transition configurations. By contrast, the melt from which the system was quenched would have many configurations, which upon quenching would be projected onto the low-temperature energy landscape. Thus, as $T \to T_K$, $W^{\ddagger}_{rlx}/W_{nonerg\ l}$ = few/many $\to 0$, and therefore $\Delta S^{\ddagger}_{rlx} \to -\infty$. At the high-temperature limit for viscous relaxation, the liquid's critical point T_c, there is essentially no differentiation between the relaxed, nonrelaxed, or transition configurations of the system. Thus, as $T \to T_c$, $W^{\ddagger}_{rlx}/W_{nonerg\ l}$ = many/many $\to 1$, and therefore $\Delta S^{\ddagger}_{rlx} \to 0$.

As a corollary to eq 15 for crystal growth, these boundary conditions can be employed to describe the temperature dependence of the entropy of activation for viscous relaxation as eq 18

$$\Delta S^{\ddagger}_{rlx}(T) = \Delta S^{\ddagger}_{rlx}\left(\frac{T_c - T}{T - T_K}\right)^{z_{rlx}} \tag{18}$$

where ΔS^{*}_{rlx} and z_{rlx} are the intrinsic, material-specific parameters that scale the magnitude of $\Delta S^{\ddagger}_{rlx}(T)$ and modulate the temperature/pressure dependence, respectively.

Notably, $W_{nonerg\ l}$ is highly sensitive to the frequency with which the liquid is quenched to the non-relaxed, nonergodic state. A more abruptly quenched liquid (large ΔT or high-frequency perturbation) will exhibit an increased $W_{nonerg\ l}$, and thus a more negative $\Delta S^{\ddagger}_{rlx}(T)$, shifting the $\eta(T)$ curve to higher temperature. This is the origin of the well-known time−temperature superposition of viscosity and the glass transition,[37,39] which we previously demonstrated is reasonably modeled with the z_{rlx} parameter.[36]

An equivalent Adam−Gibbs cooperativity term is used to describe the enthalpy of activation for viscous relaxation, and the Maxwell material model[94,95] is used to identify the prefactor to yield the TZT of viscous relaxation, TZT_{rlx}, as eq 19

$$\frac{1}{\eta} = \frac{4\pi}{v_s^2 \rho}\frac{k_B T}{h}\exp\left(\frac{-\Delta H^{*}_{rlx}}{R(T - T_K)}\right)\exp\left(\frac{\Delta S^{*}_{rlx}}{R}\left(\frac{T_c - T}{T - T_K}\right)^{z_{rlx}}\right) \tag{19}$$

where v_s is the speed of sound in the liquid, and ρ is the density of the melt.[11] This expression was shown to accurately describe the temperature-dependent viscosity from T_g to T_c of more than seventy materials.

Notably, the correlation between ΔS^{*}_{rlx} and z_{rlx} is not as high as the corresponding correlation of crystallization activation parameters; nevertheless, the general trend of the correlation persists. This may suggest that for viscous relaxation, $1/z_{rlx}$ is related to $\ln(W_{nonerg\ l}/W^{\ddagger}_{rlx})$ of the intrinsic relaxing units. As such, a highly cooperative material likely will exhibit less difference between the configurations of the intrinsic relaxing units of the nonergodic and relaxed states, and thus, the $W_{nonerg\ l}/W^{\ddagger}_{rlx}$ ratio should approach 1 resulting in a small ΔS^{*}_{rlx} and large z_{rlx} parameter. By contrast, a system exhibiting lower cooperativity will most likely have significantly more configurations accessible to the intrinsic relaxing units of the nonergodic state such that $W_{nonerg\ l}/W^{\ddagger}_{rlx}$ becomes greater than 1, resulting in a larger value of ΔS^{*}_{rlx} and smaller z_{rlx} parameter.

The primary distinction between the expressions for TZT_c and TZT_{rlx} is the inverse temperature dependence of their entropy of activation. Comparative plots of the temperature-dependent $\Delta H^{\ddagger}(T)$ and $-T\Delta S^{\ddagger}(T)$, analogous to those in Figure 3, for both crystal growth rate and viscous relaxation for diopside and SiO_2 are given in Figure 8, based on their TZT_{rlx} parameters given in Table 2.

Immediately apparent from these plots, the temperature-dependence curves of the entropic contribution to the free energy of activation of relaxation, $-T\Delta S^{\ddagger}_{rlx}(T)$, and the

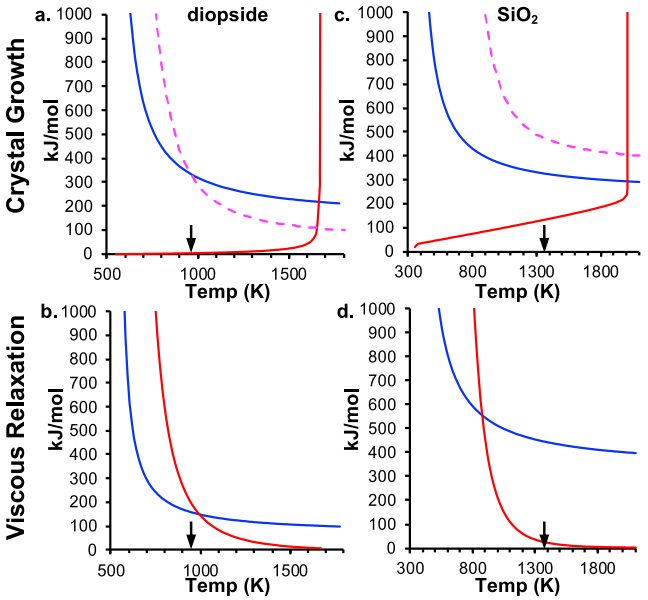

Figure 8. Temperature-dependent enthalpic $\Delta H^{\ddagger}(T)$ (blue) and entropic $-T\Delta S^{\ddagger}(T)$ (red) curves for crystallization and viscous relaxation for diopside (a,b) and SiO_2 (c,d) Purple dashed lines are the free energy of activation for relaxation, $\Delta G^{\ddagger}_{rlx} = (\Delta H^{\ddagger}_{rlx} - T\Delta S^{\ddagger}_{rlx})$. Black arrows indicate the glass transition temperature for each material.

https://dx.doi.org/10.1021/acs.jpcc.0c03003
J. Phys. Chem. C 2020, 124, 18724−18740

Table 2. TZT_{rlx} Parameters

compound	T_c (K)	T_K (K)	$v_s^2\rho$ (GPa)	ΔH^*_{rlx} (kJ/mol)	ΔS^*_{rlx} (J/mol·K)	z_{rlx}	references
$CaO{\cdot}MgO{\cdot}2SiO_2$ (diopside)	2400	534	24.3	68.3	−10.8	2.35	10
SiO_2	5400	352	36.7	322	−0.03	4.58	96

enthalpic barriers of both relaxation and crystallization, $\Delta H^{\ddagger}_{rlx}(T)$ and $\Delta H^{\ddagger}_{c}(T)$, all exhibit a common shape. Thus, with an appropriate scaling term, the free energy of activation for relaxation, $\Delta G^{\ddagger}_{rlx} = \Delta H^{\ddagger}_{rlx} - T\Delta S^{\ddagger}_{rlx}$, purple dashed line of Figure 8a,c, can be similar valued to the crystallization $\Delta H^{\ddagger}_{c}(T)$ over a significant part of the temperature range where crystal growth rates are measured. At lower temperatures, the crystallization $\Delta S^{\ddagger}_{c}(T)$ is relatively temperature independent and as such could be part of the scaling term. Thus, at temperatures moderately below T_{max}, the activation barrier for viscous relaxation and the rate of crystal growth appear to be correlated, that is the origin of the $u_{kin} \propto \eta$ assumption. By contrast, the entropic barrier to crystallization, $-T\Delta S^{\ddagger}_{c}(T)$, begins to dominate the free energy of activation for crystallization with increasing temperature, reaching an infinite discontinuity at T_m. The temperature dependence of the entropy of activation of crystallization is thus responsible for the limiting maximum crystallization rate at T_{max} and corresponding decoupling of the rates of crystal growth and viscous relaxation at higher temperature. Note that this temperature-dependent entropic activation barrier of the TZT_c model contrasts standard models, which inappropriately introduce the thermodynamic driving force term to control the kinetics of the crystal growth rate at higher temperatures (less undercooling).

Also apparent from Figure 8b,d is that with deeper undercooling, the entropic contribution to the free energy of activation for relaxation, $-T\Delta S^{\ddagger}_{rlx}(T)$, increases more rapidly with decreasing temperature than does the enthalpic contribution, $\Delta H^{\ddagger}_{rlx}(T)$. As a result, at low temperature, $-T\Delta S^{\ddagger}_{rlx}(T)$ becomes rate controlling for viscous relaxation. There is no corresponding contribution to the activation barrier for crystallization. Thus, the increasing influence of $-T\Delta S^{\ddagger}_{rlx}$ at low temperature likely is the origin of the apparent low-temperature decoupling of the rates of crystal growth and viscous relaxation. Notably, based on TZT_{rlx} for diopside, the $-T\Delta S^{\ddagger}_{rlx}(T)$ and $\Delta H^{\ddagger}_{rlx}(T)$ curves cross at 990 K, which is close to the decoupling temperatures T_D = 1040 K proposed by Schmelzer et al.[9] and 1100 K proposed by Cassar et al..[10] No such standard-model decoupling of the crystal growth and viscosity is observed for the strong network SiO_2, consistent with the observation that the $-T\Delta S^{\ddagger}_{rlx}(T)$ term does not become significant until below the glass transition temperature where no crystal growth rate data is reported. The onset of the dominating entropic activation at low temperature also explains the reported decoupling of VFT-described viscosity from the Stokes−Einstein/Eyring relationship, as the VFT expression[22−24] does not differentiate enthalpic and entropic effects.

7. SUMMARY AND CONCLUSIONS

As demonstrated by analysis of a diverse set of organic molecular and inorganic network materials, the TZT of crystallization, TZT_c, provides a superior fit to experimental crystal growth-rate data when compared to standard models. The TZT_c, a single model that accurately describes crystal growth rates for diverse materials, for the first time, provides a platform with which to evaluate molecular functional group and crystal structure effects on the activation barriers for crystal growth.

As revealed by the functional-group dependence of the crystallization rate of a series of ortho-substituted benzenes and two examples of poly-alcohols, the introduction of molecular degrees of freedom has a greater effect on crystal growth rates than does the introduction of strong hydrogen-bonding functional groups. The TZT_c also reveals that the isostructural layered $A_2O{\cdot}nSiO_2$ (A = Li, n = 2,3 and A = Na, n = 2) materials crystallize with a common activation process, distinct from the more isotropic $Na_2O{\cdot}3SiO_2$. Furthermore, systems with highly mobile cations, such as the proton-conducting $[Zn(OH_2)_6][ZnCl_4]$ and the Li^+-conducting $LiPO_3$, exhibit very large negative entropies of activation, consistent with the need to restrict ionic mobility in order to construct the long-range order of a crystalline lattice. These, and more examples, demonstrate chemical insight that can be revealed and/or predicted based on the TZT_c analysis of crystallization reactions.

Not only is experimental crystallization data better fit with the TZT_c model than with standard models, but all of the TZT_c parameters, the enthalpic, ΔH^*_c, and entropic, ΔS^*_c, activation parameters, and the cooperativity/temperature-dependence modulating parameter, z_c, have a sound physical−chemical basis. Notably, for a non-cooperative crystallizing system with z_c = 0, which removes the entropic temperature dependence, and at high temperatures, or when T_K = 0, where the enthalpic temperature dependence $T/(T - T_K) \rightarrow 1$, the TZT_c expression collapses to Eyring's expression of the transition state theory.

Unlike the standard models, TZT_c does not invoke equilibrium concepts to describe the microscopically irreversible process of crystallization nor does it imply particle diffusion to or particle attachment to/detachment from an arbitrarily defined liquid/crystal interface. Instead, TZT_c, consistent with well-established knowledge of the common short- and intermediate-range order of liquids and solids, is based on an understanding that crystallization must be an ensemble, rather than an individual particle, based process. Corresponding application of cooperative/ensemble-based principles to describe viscous relaxation, the TZT_{rlx}, also provides explanation of the apparent decoupling of crystal growth rates and viscous relaxation, clearly demonstrating that viscous relaxation is not part of the activation process for crystal growth.

AUTHOR INFORMATION

Corresponding Author

James D. Martin − *Department of Chemistry, North Carolina State University, Raleigh, North Carolina 27539, United States*; orcid.org/0000-0001-7414-2683; Phone: 919-515-3402; Email: Jim_Martin@NCSU.EDU

Authors

Berkley G. Hillis − *Department of Chemistry, North Carolina State University, Raleigh, North Carolina 27539, United States*

https://dx.doi.org/10.1021/acs.jpcc.0c03003
J. Phys. Chem. C 2020, 124, 18724−18740

Feier Hou − *Department of Chemistry, North Carolina State University, Raleigh, North Carolina 27539, United States;* orcid.org/0000-0002-6314-0129

Complete contact information is available at: https://pubs.acs.org/10.1021/acs.jpcc.0c03003

Notes

The authors declare no competing financial interest.

■ ACKNOWLEDGMENTS

This work was supported by National Science Foundation via contract DMR-1709370.

■ ABBREVIATIONS

TZT_c, transition zone theory of crystallization; T_{max}, temperature of the maximum observed crystal growth rate; v, U, v_{pb}, velocity of solidification; C, a constant related to the heat of fusion and the thickness of a layer of molecules at the interface; V or η, viscosity; s, amount of supercooling; Q, heat of activation or of fusion; T_s or T_m, melting temperature; R, the gas constant; μ, chemical potential; F, size of crystal face; ρ, a free energy of growth boundaries, also density; f, a function describing attachment sites; D, diffusion coefficient; ΔG, free-energy difference; λ or δ, a jump distance, λ also corresponds to a characteristic wavelength of vibrations leading to crystal growth equivalent to 2× average lattice constant; k_B, Boltzmann's constant; γ, specific surface energy; V_m, molar volume; N, number of formula unit per unit area; Γ, the gamma function; U_R or u_{kin}, reduced growth rate; ξ, a viscosity correction parameter; T_D, viscosity-crystal growth decoupling temperature; E_a or U', an activation energy; VFT, Volger−Folcher−Tamman; $\Delta G^{\ddagger}$, free energy of activation; H, enthalpy; k_f and k_r, forward and reverse rate constants; r_{vdW}, van der Waals radius; l, mean free path; v, average velocity, also used to describe frequency; τ_0, period of oscillation; T_K, Kauzmann temperature; h, Planck's constant; W, number of configurations; S, entropy; ΔS^* and ΔH^*, intrinsic entropic and enthalpic contribution to the temperature-dependent activation entropy and enthalpy, respectively; z, a parameter to modulate the temperature-dependent cooperativity of a system; OTP, *o*-terphenyl; CZX-1, $[HNMe_3][CuZn_5Cl_{12}]$; ROY, red, yellow, and orange polymorphic compound 5-methyl-2-[(2-nitrophenyl)amino]-3-thiophenecarbonitrile; m, fragility; TZ, transition zone; T_c, the critical point; v_s, speed of sound in the medium; T_g, glass transition temperature; TZT_{rlx}, transition zone theory of viscous relaxation

■ REFERENCES

(1) Bohm, J. The History of Crystal Growth. *Acta Physiol. Hung.* **1985**, *57*, 161−178.
(2) Kepler, J., "Strena seu de nive sexangular." Frankfurt, Germany: Tampach, 1611. *Reprinted in Gesammelte Werke*; Caspar, M., Hammer, F., Eds.; Clarendon Press: Oxford, England, 1966; Vol. *4*.
(3) Tammann, G. Uber die Abhängigkeit der Zahl der Kerne, welches ich in verschiedenen unterküyotehn Flüssigkeiten bilden, von der Temperatur. *Z. Physiol. Chem.* **1898**, *25*, 441−479.
(4) Wilson, H. W. XX. On the velocity of solidification and viscosity of super-cooled liquids. *Philos. Mag.* **1900**, *50*, 238−250.
(5) Frenkel, J. Note on a Relation Between the Speed of Crystallization and Viscosity. *Phys. Z. Sowjetunion* **1932**, *1*, 498−500.
(6) Gibbs, J. W. On the Equilibrium of Heterogeneous Substances. *Trans. Conn. Acad. Arts Sci.* **1878**, *16*, 343−524.
(7) Becker, R.; Döring, W. Kinetische Behandlung der Keimbildung in übersättigten Dämpfen. *Ann. Phys.* **1935**, *416*, 719−752.
(8) Ediger, M. D.; Harrowell, P.; Yu, L. Crystal growth kinetics exibit a fragility-dependent decoupling from viscosity. *J. Chem. Phys.* **2008**, *128*, 034709.
(9) Schmelzer, J. W. P.; Abyzov, A. S.; Fokin, V. M.; Schick, C.; Zanotto, E. D. Crystallization in glass-forming liquids: Effects of decoupling of diffusion and viscosity on crystal growth. *J. Non-Cryst. Solids* **2015**, *429*, 45−53.
(10) Cassar, D. R.; Rodrigues, A. M.; Nascimento, M. L. F.; Zanotto, E. D. The diffusion coefficient controlling crystal growth in a silicate glass-former. *Int. J. Appl. Glass Sci.* **2018**, *9*, 373−382.
(11) Hou, F.; Martin, J. D.; Dill, E. D.; Folmer, J. C. W.; Josey, A. A. Transition Zone Theory of Crystal Growth and Viscosity. *Chem. Mater.* **2015**, *27*, 3526−3532.
(12) Kauzmann, W. The nature of the glassy state and the behavior of liquids at low temperatures. *Chem. Rev.* **1948**, *43*, 219−256.
(13) Adam, G.; Gibbs, J. H. On the Temperature dependence of Cooperative Relaxation Properties in Glass-Forming Liquids. *J. Chem. Phys.* **1965**, *43*, 139−146.
(14) Eyring, H. The activated complex in chemical reactions. *J. Chem. Phys.* **1935**, *3*, 107−115.
(15) Nascimento, M. L. F.; Zanotto, E. D. Does viscosity describe the kinetic barrier for crystal growth from the liquidus to the glass transition? *J. Chem. Phys.* **2010**, *133*, 174701.
(16) Volmer, M.; Marder, M. Zur Theorie de linearen Kristallisationsgeschwindigkeit unterkühlter fester Modifikationen. *Z. Physiol. Chem.* **1931**, *154*, 97−112.
(17) Volmer, M. ""Zum Problem des Kristallwachstumus. *Z. Physiol. Chem.* **1922**, *102*, 267−275.
(18) Kossel, W. "Zur Theorie des Kristallwachstums.". *Z. Phys. Chem.* **1927**, *126*, 135−143.
(19) Turnbull, D.; Fisher, J. C. Rate of Nucleation in Condensed Systems. *J. Chem. Phys.* **1949**, *17*, 71−73.
(20) Cahn, J. W. Theory of Crystal Growth and Interface Motion in Crystalline Materials. *Acta Metall.* **1960**, *8*, 554−562.
(21) Jackson, K. A.; Uhlmann, D. R.; Hunt, J. D. On the Nature of Crystal Growth from the Melt. *J. Cryst. Growth* **1967**, *1*, 1−36.
(22) Fulcher, G. S. Analysis of Recent Measurements of the Viscosity of Glasses. *J. Am. Ceram. Soc.* **1925**, *8*, 339−355.
(23) Tammann, G.; Hesse, W. Z. Die Abhängigkeit der Viscosität von der Temperature bie unterkühlten Flüssigkeiten. *Z. Anorg. Allg. Chem.* **1926**, *156*, 245−257.
(24) Vogel, H. Das Temperaturabhangigkeitsgesetz der Viscosität von Flüssigkeiten. *Phys. Z.* **1921**, *22*, 645−646.
(25) Schönhals, A.; Kremer, F.; Hofmann, A.; Fischer, E. W. Anomalies in the scaling of the α-relaxation studied by dielectric spectroscopy. *Physica A* **1993**, *201*, 263−269.
(26) Stickel, F.; Fischer, E. W.; Richert, R. Dynamics of glass-forming liquids. II. Detailed comparison of dielectric relaxation, dc-conductivity and viscosity data. *J. Chem. Phys.* **1996**, *104*, 2043−2055.
(27) Mauro, J. C. Through a Glass, Darkly: Dispelling Three Common Misconceptions in Glass Science. *Int. J. Appl. Glass Sci.* **2011**, *2*, 245−261.
(28) Kirkpatrick, R. J. Crystal Growth from the Melt: A Review. *Am. Mineral.* **1975**, *60*, 798−814.
(29) Chernov, A. A. Notes on interface growth kinetics 50 years after Burton, Cabrera and Frank. *J. Cryst. Growth* **2004**, *264*, 499−518.
(30) Skripov, V. P.; Galashev, A. E. The Structure of Simple Liquids. *Russ. Chem. Rev.* **1983**, *52*, 97−116.
(31) Wright, A. C. Neutron scattering from vitreous silica. V. The structure of vitreous silica: What have we learned from 60 years of diffraction studies? *J. Non-Cryst. Solids* **1994**, *179*, 84−115.
(32) Salmon, P. S.; Martin, R. A.; Mason, P. E.; Cuello, G. J. Topological versus chemical ordering in network glasses at intermediate and extended length scales. *Nature* **2005**, *435*, 75−78.
(33) Martin, J. D.; Goettler, S. J.; Fossé, N.; Iton, L. Designing Intermediate Range Order in Amorphous Materials. *Nature* **2002**, *419*, 381−384.

(34) How, J. M. "Direct observation of order in the liquid at a solid−liquid interface by high-resolution transmission electron microscopy. *Philos. Mag. A* **1996**, *74*, 761−775.
(35) Algra, R. E.; Vonk, V.; Wermeille, D.; Szweryn, W. J.; Verheijen, M. A.; van Enckevort, W. J. P.; Bode, A. A. C.; Noorduin, W. L.; Tancini, E.; de Jong, A. E. F.; Bakkers, E. P. A. M.; Vlieg, E. Formation of Wurtzite InP Nanowires Explained by Liquid-Ordering. *Nano Lett.* **2011**, *11*, 44−48.
(36) Sangroniz, L.; Cavallo, D.; Müller, A. J. Self-Nucleation Effects on Polymer Crystallization. *Macromolecules* **2020**, *53*, 4581.
(37) Martin, J. D.; Hou, F. Transition zone theory of the glass transition. *J. Non-Cryst. Solids* **2018**, *491*, 24−33.
(38) Androsch, R.; Schick, C. Interplay between the relaxation of the glass of random l/D-lactide copolymers and homogeneous crystal nucleation: evidence for segregation of chain defects. *J. Phys. Chem. B* **2016**, *120*, 4522−4528.
(39) An, H.; Li, X.; Geng, Y.; Wang, Y.; Wang, X.; Li, L.; Li, Z.; Yang, C. Shear induced conformational ordering, relaxation, and crystallization of isotactic polypropylene. *J. Phys. Chem. B* **2008**, *112*, 12256−12262.
(40) Williams, M. L.; Landel, R. F.; Ferry, J. D. The temperature dependence of relaxation mechanisms in amorphous polymers and other glass-forming liquids. *J. Am. Chem. Soc.* **1955**, *77*, 3701−3707.
(41) Hou, F.; Martin, J. D. Isotope Effects Reveal the Template Influence on the Intrinsic Mechanism of Crystal Growth of a Metal Halide Network. *J. Phys. Chem. C* **2019**, *123*, 7475−7485.
(42) Schneider, T.; Brout, R.; Thomas, H.; Feder, J. Dynamics of the Liquid-Solid Transition. *Phys. Rev. Lett.* **1970**, *25*, 1423−1426.
(43) Thompson, C. V.; Spaepen, F. On the Approximation of the Free Energy Change on Crystallization. *Acta Metall.* **1979**, *27*, 1855−1859.
(44) Hillis, B. G.; Losey, B. P.; Weng, J.; Ghaleb, N.; Hou, F.; Martin, J. D. From Rate Measurements to Mechanistic Data for Condensed Matter Reactions: A case study using the crystallization of $[Zn(OH_2)_6][ZnCl_4]$. *Crystals* **2017**, *7*, 11.
(45) Wagstaff, F. E. Crystallization and Melting Kinetics of Cristobalite. *J. Am. Ceram. Soc.* **1969**, *52*, 650−654.
(46) Wagstaff, F. E. Crystallization kinetics of internally nucleated vitreous silica. *J. Am. Ceram. Soc.* **1968**, *51*, 449−453.
(47) Vergano, P. J.; Uhlmann, D. R. Crystallization kinetics of germanium dioxide: the effect of stoichiometry on kinetics. *Phys. Chem. Glasses* **1970**, *11*, 30−38.
(48) Ota, R.; Mishima, N.; Wakasugi, T.; Fukunaga, J. Nucleation kinetics of a $Li_2O{\cdot}2SiO_2$ glass based on a liquid model. *J. Mater. Sci.* **1999**, *34*, 5937−5941.
(49) Burgner, L. L.; Weinberg, M. C. An assessment of crystal growth behavior in lithium disilicate glass. *J. Non-Cryst. Solids* **2001**, *279*, 28−43.
(50) Barker, M. F.; Wang, T.; James, P. F. Nucleation and growth kinetics of lithium disilicate and lithium metasilicate in lithia-silica glasses. *Phys. Chem. Glasses* **1988**, *29*, 240−248.
(51) James, P. F. Kinetics of crystal nucleation in silicate glasses. *J. Non-Cryst. Solids* **1985**, *73*, 517−540.
(52) Matusita, K.; Sakka, S.; Maki, T.; Tashiro, M. Study on crystallization of glass by differential thermal analysis. Effect of added oxide on crystallization of Li_2O-SiO_2. *J. Mater. Sci.* **1975**, *10*, 94−100.
(53) Schmidt, A.; Frischat, G. H. Atomic force microscopy of early crystallisation stages in Li2O.2SiO2 glasses. *Phys. Chem. Glasses* **1997**, *38*, 161−166.
(54) Fokin, V. M.; Potapov, O. V.; Zanotto, E. D.; Spiandorello, F. M.; Ugolkov, V. L.; Pevzner, B. Z. Mutant crystals in $Na_2{\cdot}2CaO{\cdot}3SiO_2$ glasses. *J. Non-Cryst. Solids* **2003**, *331*, 240−253.
(55) Zanotto, E. D.; Leite, M. L. G. The nucleation mechanism of lithium disilicate glass revisited. *J. Non-Cryst. Solids* **1996**, *202*, 145−152.
(56) Gonzalez-Oliver, C. J. R.; Johnson, P. S.; James, P. F. Influence of water content on the rates of crystal nucleation and growth in lithia-silica and soda-lime-silica glasses. *J. Mater. Sci.* **1979**, *14*, 1159−1169.
(57) Ogura, T.; Hayami, R.; Kadota, M. Kinetics and mechanism of crystallization of lithium silicate glasses. *J. Ceram. Assn. Japan* **1968**, *76*, 33−40.
(58) Ghoneim, N. Crystallization of lithium trisilicate glasses. *Trans. J. Br. Ceram. Soc.* **1979**, *78*, 15.
(59) Meiling, G.; Uhlmann, D. R. Crystallization and melting kinetics of sodium disilicate. *Phys. Chem. Glasses* **1967**, *8*, 62−68.
(60) Sherer, G. W.; Uhlmann, D. R. Crystallization kinetics of $Na_2O{\cdot}3SiO_2$. *J. Cryst. Growth* **1975**, *29*, 12−18.
(61) Neiman, T. S.; Yinnon, H.; Uhlmann, D. R. Crystallization Kinetics of Lead Metasilicate. *J. Non-Cryst. Solids* **1982**, *48*, 393−403.
(62) Reinsch, S.; Nascimento, M. L. F.; Müller, R.; Zanotto, E. D. Crystal growth kinetics in cordierite and diopside glasses in wide temperature ranges. *J. Non-Cryst. Solids* **2008**, *354*, 5386−5394.
(63) Kirkpatrick, R. J.; Robinson, G. R.; Hays, J. F. Kinetics of crystal growth from silicate melts: anorthite and diopside. *J. Geophys. Res.* **1976**, *81*, 5715−5720.
(64) Fokin, V. M.; Yuritsyn, N. S.; Zanotto, E. D. *"Nucleation and crystallization kinetics in silicate glasses: theory and experiment." Nucleation Theory and Applications*; Schmelzer, J. W. P., Ed.; WileyVCH: Hoboken, NJ, 2005, pp 74−125.
(65) Zanotto, E. D. Surface Nucleation in Diopside Glass. *J. Non-Cryst. Solids* **1991**, *130*, 217−219.
(66) Klein, L.; Uhlmann, D. R. Crystallization behavior of anorthite. *J. Geophys. Res.* **1974**, *79*, 4869−4874.
(67) Avramov, I.; Gutzow, I.; Grantscharova, E. Crystallization kinetics and rheology of undercooled melts. *J. Cryst. Growth* **1988**, *87*, 305−310.
(68) Avramov, I.; Pascova, R.; Samouneva, B.; Gutzow, I. The mechanism of crystallization and dissolution of $LiPO_3$ from its melt. *Phys. Chem. Glasses* **1979**, *20*, 91−96.
(69) Magill, J. H.; Plazek, D. J. Physical Properties of Aromatic Hydrocarbons .2. Solidification Behavior of 1,3,5-Tri-Alpha-Naphthylbenzene. *J. Chem. Phys.* **1967**, *46*, 3757−3769.
(70) Scherer, G.; Uhlmann, D. R.; Miller, C. E.; Jackson, K. A. Crystallization Behavior of High-Purity Ortho-Terphenyl. *J. Cryst. Growth* **1974**, *23*, 323−330.
(71) Konishi, T.; Tanaka, H. Possible origin of enhanced crystal growth in a glass. *Phys. Rev. B: Condens. Matter Mater. Phys.* **2007**, *76*, 22020.
(72) Scherer, G.; Uhlmann, D. R. Crystallization behavior of α-phenyl o-cresol. *J. Cryst. Growth* **1972**, *15*, 1−10.
(73) Sun, Y.; Xi, H.; Ediger, M. D.; Yu, L. Diffusionless Crystal Growth from Glass Has Precursor in Equilibrium Liquid. *Phys. Chem. B.* **2008**, *112*, 661−664.
(74) Wu, T.; Yu, L. Origin of enhanced crystal growth kinetics near Tg probed with indomethacin polymorphs. *J. Phys. Chem. B* **2006**, *110*, 15694−15699.
(75) Yu, L. Growth rings in D-sorbitol spherulites: Connection to concomitant polymorphs and growth kinetics. *Cryst. Growth Des.* **2003**, *3*, 967−971.
(76) Mei, Q.; Benmore, C. J.; Weber, J. K. R. Structure of Liquid SiO_2: A Measurement by High-Energy X-ray Diffraction. *Phys. Rev. Lett.* **2007**, *98*, 057802.
(77) Andrews, J. N.; Ubbelohde, A. R. Melting and crystal structure: the melting parameters of some polyphenyls. *Proc. R. Soc. London, Ser. A* **1955**, *228*, 435−447.
(78) Debye, P.; Scherrer, P. "Interferenzen and regellos orientierten Teilchen im Röntgenlict. II". *Nachr. Ges. Wiss. Göttingen, Math.-Phys. Kl.* **1916**, *1916*, 16−26.
(79) Wilcox, R. J.; Losey, B. P.; Folmer, J. C. W.; Martin, J. D.; Zeller, M.; Sommer, R. Crystalline and Liquid Structure of Zinc Chloride Tri-hydrate: A unique ionic liquid. *Inorg. Chem.* **2015**, *54*, 1109−1119.
(80) Xu, M.; Jing, Z.; Chantel, J.; Jiang, P.; Yu, T.; Wang, Y. Ultrasonic Velocity of Diopside Liquid at High Presure and temperature: Constraints on Velocity Reduction in the Upper Mantle Due to Partial Melts. *J. Geophys. Res.: Solid Earth* **2018**, *123*, 8676−8690.

https://dx.doi.org/10.1021/acs.jpcc.0c03003
J. Phys. Chem. C 2020, 124, 18724−18740

(81) Angell, C. A. "Relaxation in liquids, polymers and plastic crystals—strong/fragile patterns and problems. *J. Non-Cryst. Solids* **1991**, *131−133*, 13−31.
(82) Hammett, L. P. The Effect of Structure upon the Reactions of Organic Compounds. Benzene Derivatives". *J. Am. Chem. Soc.* **1937**, *59*, 96−103.
(83) Headen, T. F.; Cullen, P. L.; Patel, R.; Taylor, A.; Skipper, N. T. The structures of liquid pyridine and naphthalene: the effects of heteroatoms and core size on aromatic interactions. *Phys. Chem. Chem. Phys.* **2018**, *20*, 2074−2715.
(84) Bilgram, J. H.; Dürig, U.; Wächter, M.; Seiler, P. Zone refining and structure determination of salol crystals. *J. Cryst. Growth* **1982**, *57*, 1−5.
(85) Hammond, R. B.; Jones, M. J.; Roberts, K. J.; Kutzke, H.; Klapper, H. A structural study of polymorphism in phenyl salicylate: determination of the crystal structure of a meta-stable phase from X-ray powder diffraction data using a direct space systematic search method. *Z. Kristallogr.* **2002**, *217*, 484−491.
(86) Yu, L. Polymorphism in Molecular Solids: An Extraordinary System of Red, Orange, and Yellow Crystals. *Acc. Chem. Res.* **2010**, *43*, 1257−1266.
(87) Kistenmacher, T. J.; Marsh, R. E. Crystal and molecular structure of an anti-inflammatory agent, indomethacin, 1-(p-chlorobenzoyl)-5-methoxy-2-methylindole-3-acetic acid. *J. Am. Chem. Soc.* **1972**, *94*, 1340−1345.
(88) Crowley, K. J.; Zografi, G. Cryogenic grinding of indomethacin polymorphs and solvates: assessment of amorphous phase formation and amorphous phase physical stability. *J. Pharm. Sci.* **2002**, *91*, 492−507.
(89) Zhao, J.; Gaskell, P. H.; Cluckie, M. M.; Soper, A. K. A neutron diffraction, isotopic substitution study of the structure of $Li_2O{\cdot}2SiO_2$ glass. *J. Non-Cryst. Solids* **1998**, *232−234*, 721−727.
(90) Krüger, H.; Kahlenberg, V.; Kaindl, R. Li2Si3O7: Crystal structure and Raman spectroscopy. *J. Solid State Chem.* **2007**, *180*, 922−928.
(91) Pant, A. K.; Cruickshank, D. W. J. The crystal structure of α-$Na_2Si_2O_5$. *Acta Crystallogr.* **1968**, *24*, 13−19.
(92) Kahlenberg, V.; Marler, B.; Muñoz Acevedo, J. C.; Patarin, J. Ab initio crystal structure determination of $Na_2Si_3O_7$ from conventional powder diffraction data. *Solid State Sci.* **2002**, *4*, 1285−1292.
(93) Hockicko, P.; Kudelcik, J.; Munoz, F.; Munoz-Senovilla, L. Structural and Electrical Properties of $LiPO_3$ Glasses. *Appl. Phys.* **2015**, *13*, 198−205.
(94) Oestreicher, H. L. Field and impedance of an oscillating sphere in a viscoelastic medium with an application to biophysics. *J. Acoust. Soc. Am.* **1951**, *23*, 707−714.
(95) Chen, K.; Yao, A.; Zheng, E. E.; Lin, J.; Zheng, Y. Shear Wave Dispersion Ultrasound Vibrometry Based on a Different Mechanical Model for Soft Tissue Characterization. *J. Ultrasound Med.* **2012**, *31*, 2001−2011.
(96) Doremus, R. H. Viscosity of silica. *J. Appl. Phys.* **2002**, *92*, 7619−7629.

https://dx.doi.org/10.1021/acs.jpcc.0c03003
J. Phys. Chem. C 2020, 124, 18724−18740